Construction and First Evaluation of the HiZ-GUNDAM/EAGLE Optics System Prototype

Hatsune Goto[a], Isshin Nagataka[a], Daisuke Yonetoku[a], Daiki Ishi[b], Yoshitomo Maeda[b], Hsien-Chieh Shen[c], Ryuji Kondo[a], Akito Kutsumi[a], Hiroshi Tomida[b], Makoto Arimoto[a], Shutaro Ueda[a], Tatsuya Sawano[a], Keito Watanabe[d], Haruaki Niinuma[d], Takumi Togashi[d], Rinon Kageyama[e], Tatsuro Kanenaga[a], Tenshin Otsuka[a], Junpei Kuwabara[a], Motoko Serino[f], Yuta Yamamoto[g], Kanta Yagi[g], Kaita Nakahashi[f], Kenta Kanoh[f], Satoshi Sugita[f], Yuya Nagase[a], Shuichi Gunji[d], Akihiro Doi[b], Hideo Matsuhara[b]

Kanazawa University[a], ISAS/JAXA[b], RIKEN[c], Yamagata University[d], Tokyo City Univercity[e], Aoyama Gakuin University[f], Kwansei Gakuin University[g]

2025 18th November

Multi-messenger Astrophysics Annual Conference

EAGLE and its Optics System

❖Configuration

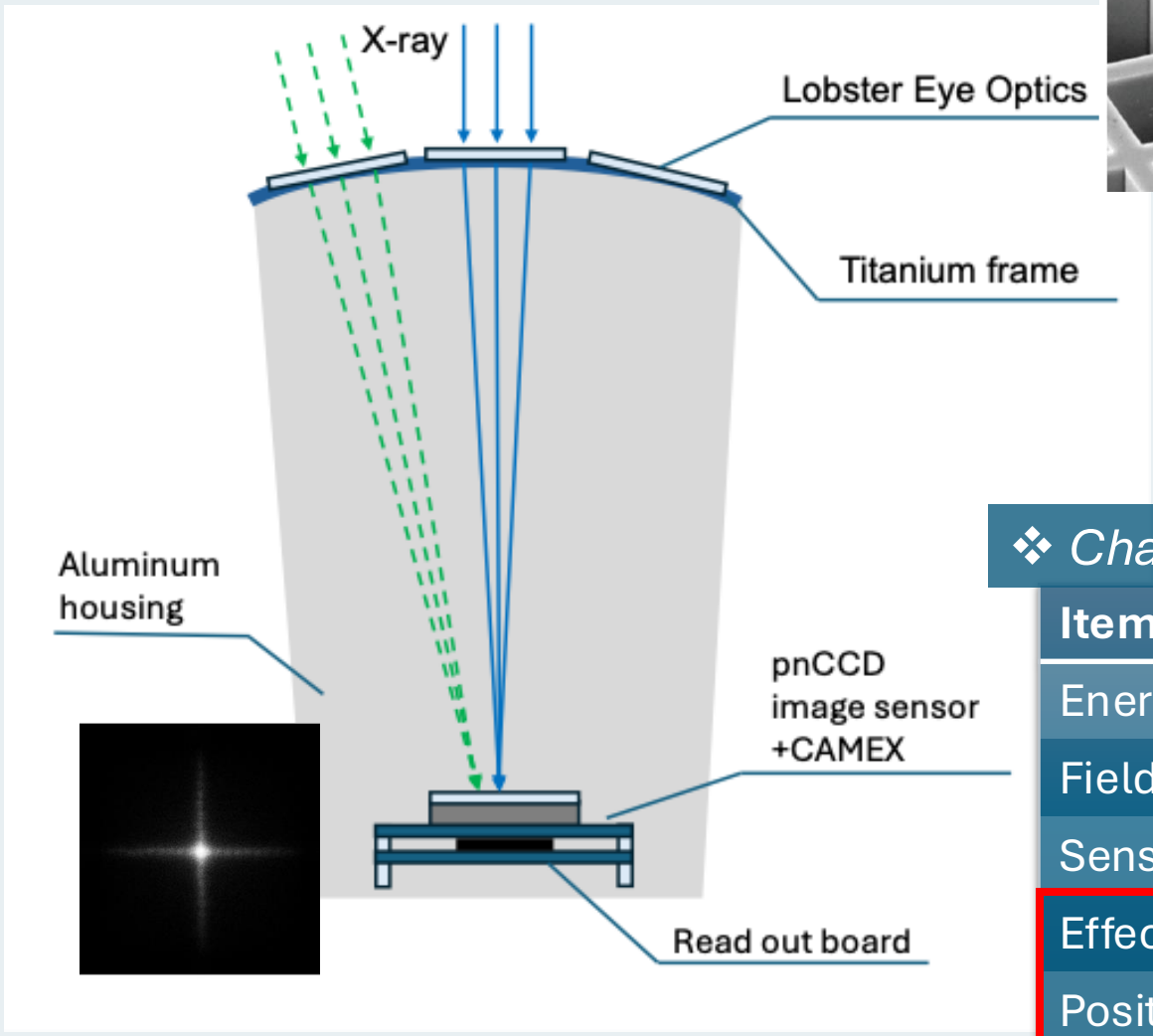

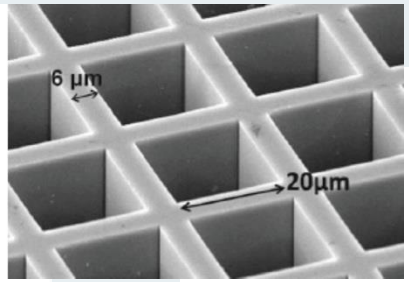

Micro-Pore type Optics(**MPO**)

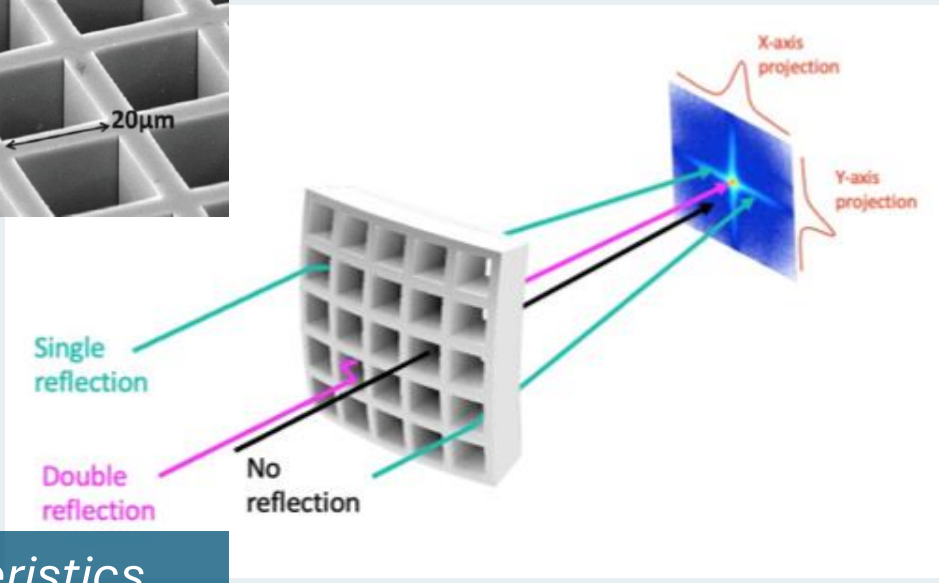

❖ *Characteristics*

Items	Parameters
Energy band (keV)	0.4 – 4 keV
Field of View	0.5 steradian
Sensitivity	= 4e-10 (erg/cm2/s)For 100 sec
Effective area	To be investigated
Position accuracy	3 arcmin at 2σ

Goal of construction

Main issue of the Construction

❖ **Angle tuning of MPO segments**

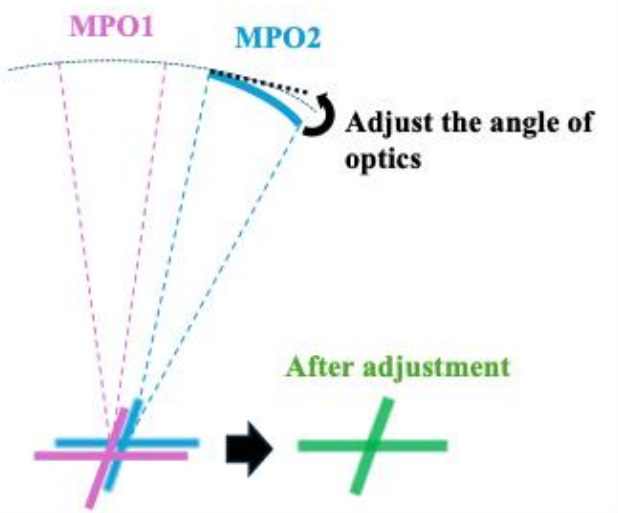

👍 Localization accuracy

image
Y axis

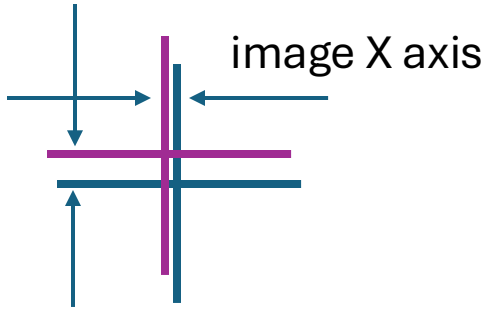

➢ FY 2023

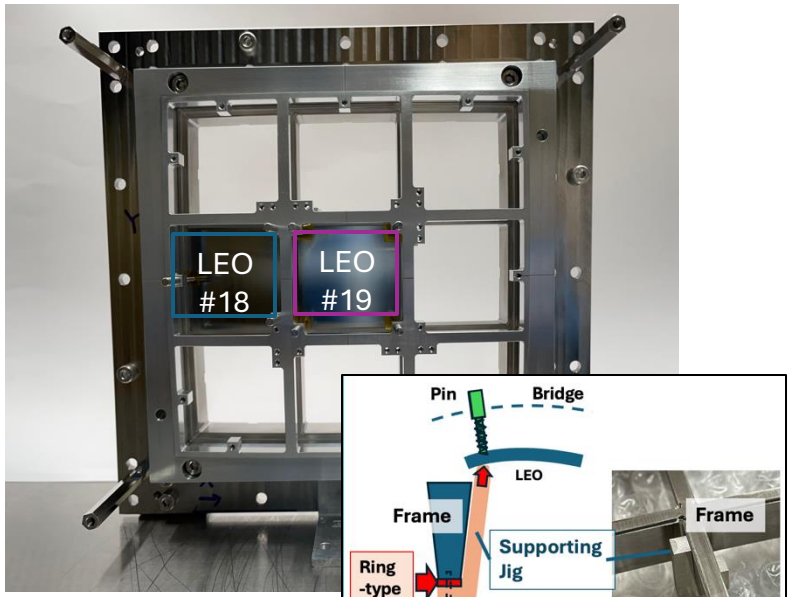

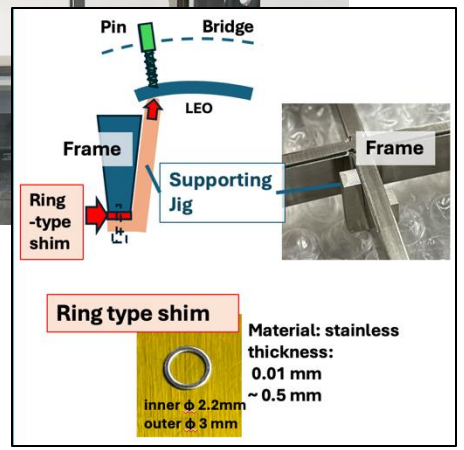

- Manual angle adjustment with thin metal plate
- Angle tuning for only X axis
  2 MPO, 2 weeks

➢ FY 2025

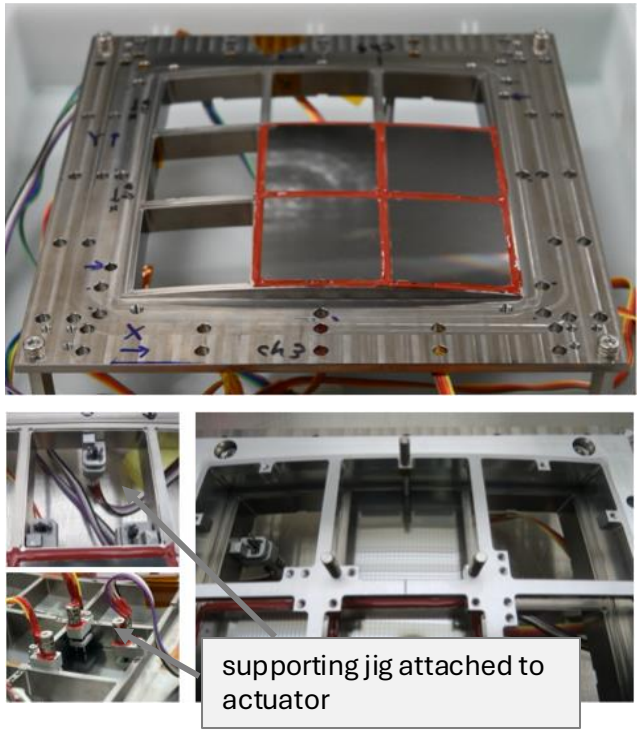

- **Automatic angle adjustment** in vacuum environment
- Angle tuning for X and Y axis
  4 MPO, 1 days

Construction / Evaluation in ISAS/JAXA

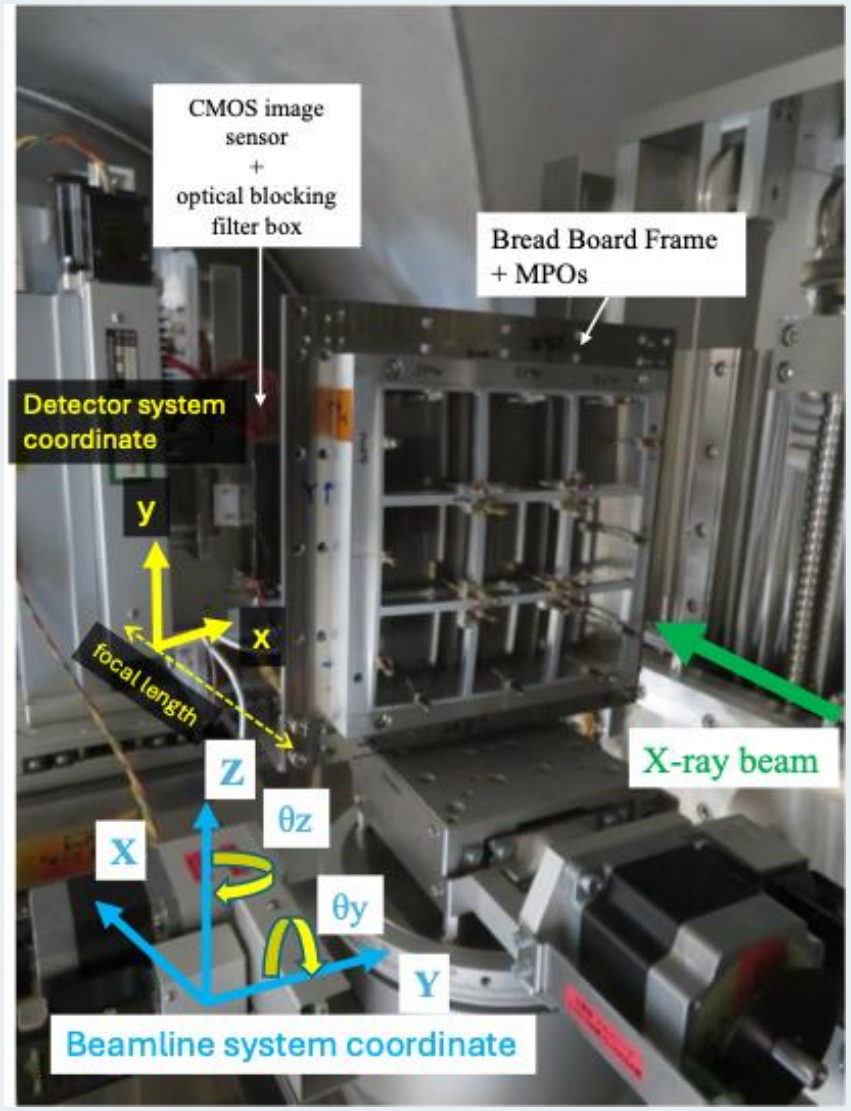

@27 m X-ray beamline in ISAS/JAXA

❖**Construction of Optics System**

25 August- 7 September, 2025 …selection, angle tuning of each segment

❖**Evaluation of Optics System**

13-26 September, 2025 …measure localization accuracy and effective area

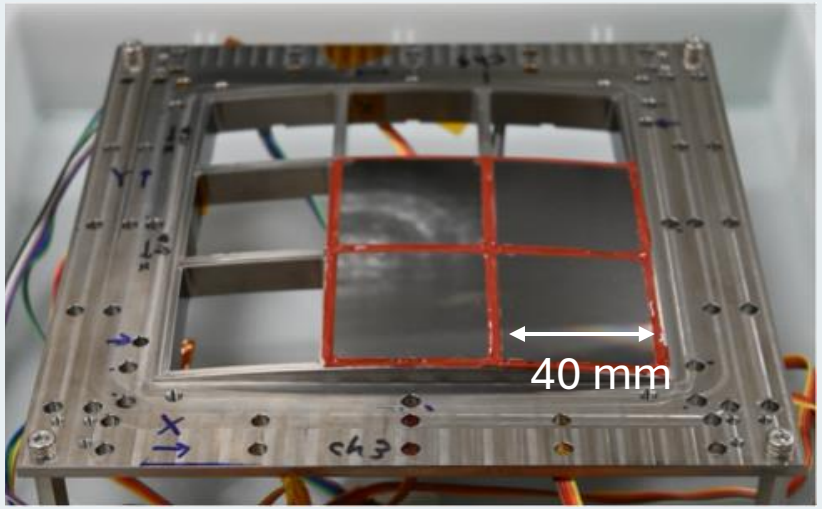

Optics System Construction

See Isshin Nagataka's poster

Selection of MPO Segments

- Best Focal Length

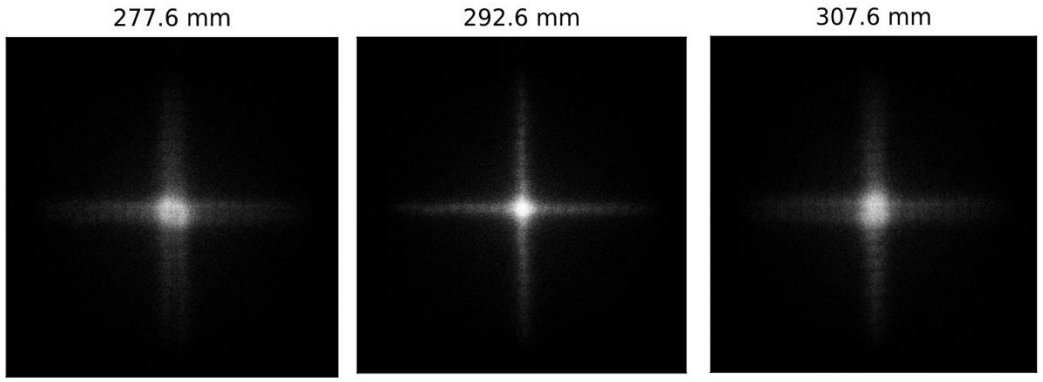

- Distortion in Angular Response

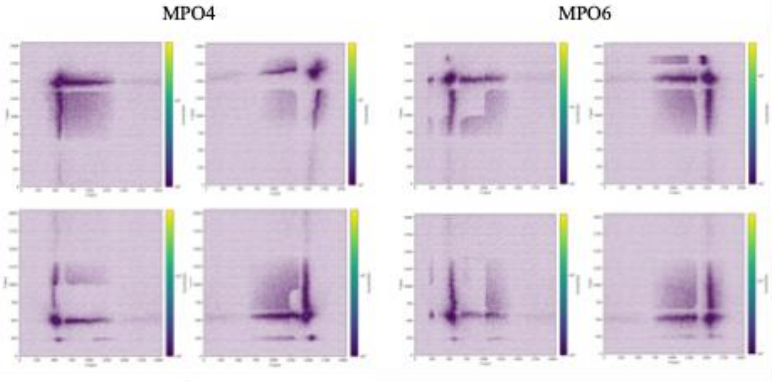

Adjustment of Segment Angle

Selected best 4 from 7 MPO segments

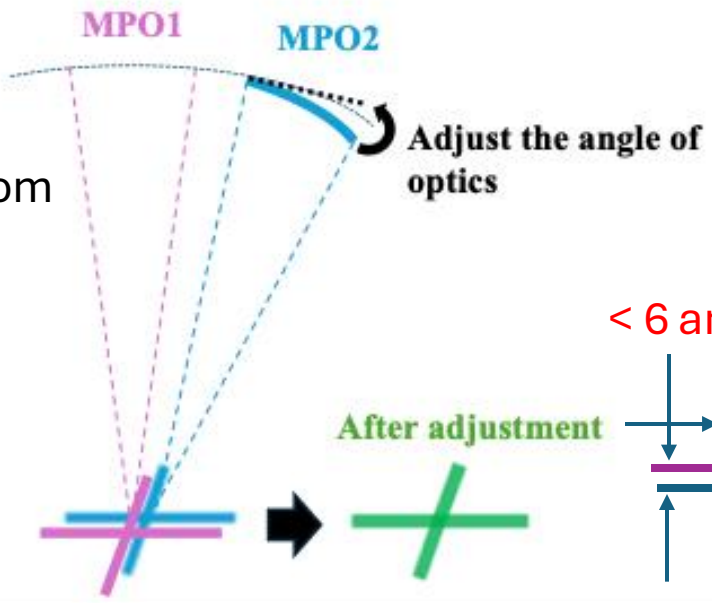

< 6 arcmin precision

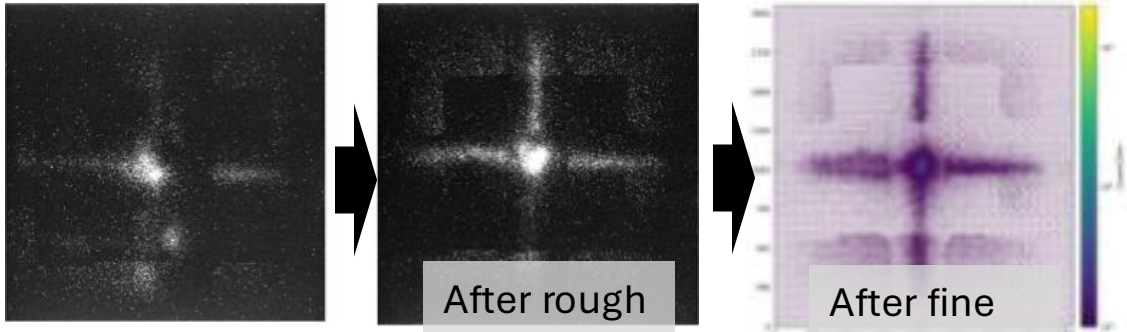

Evaluation of Optics System

Testing Localization Accuracy

❖ Rotation of Frames and Detectors

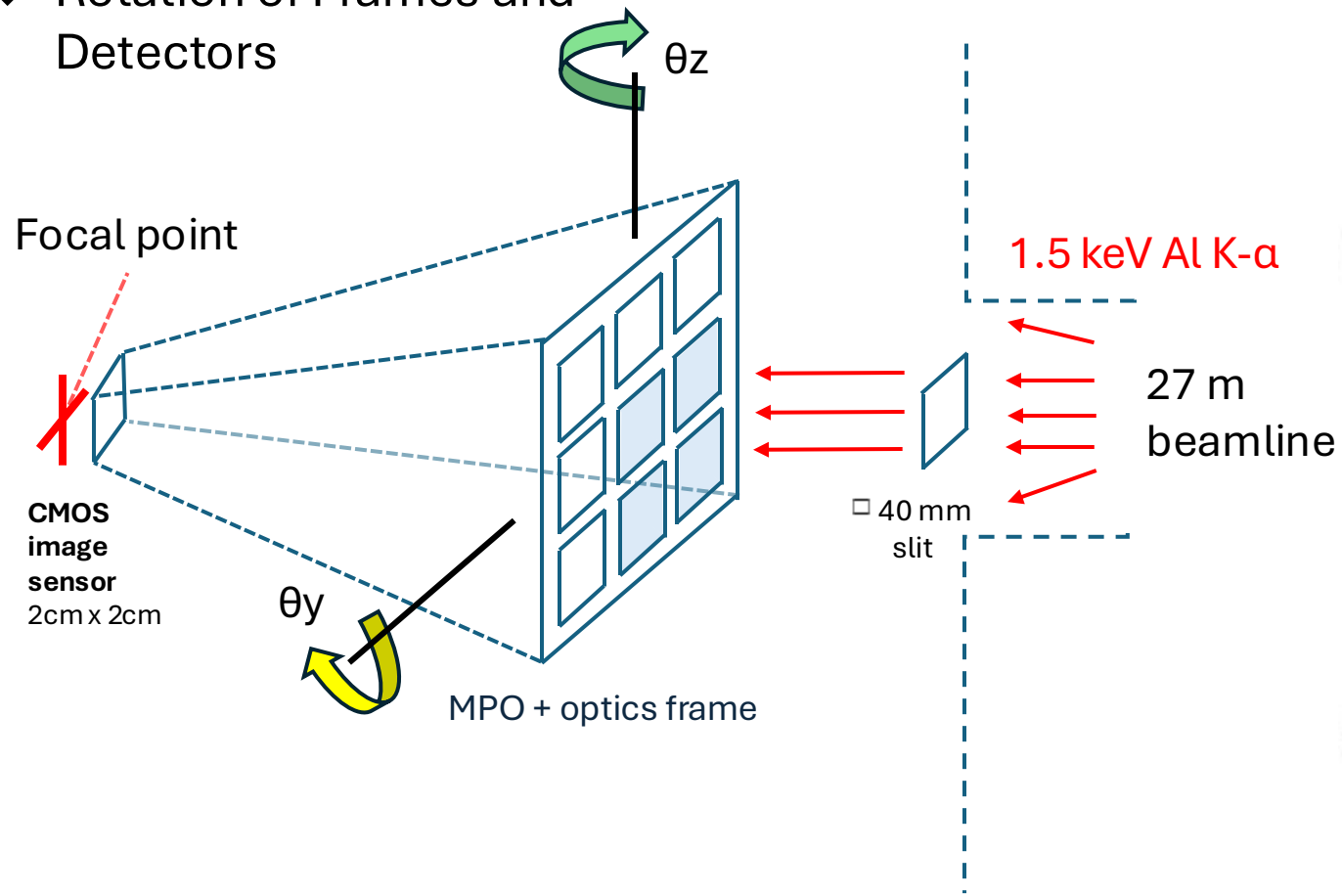

❖ Detection of Focal point

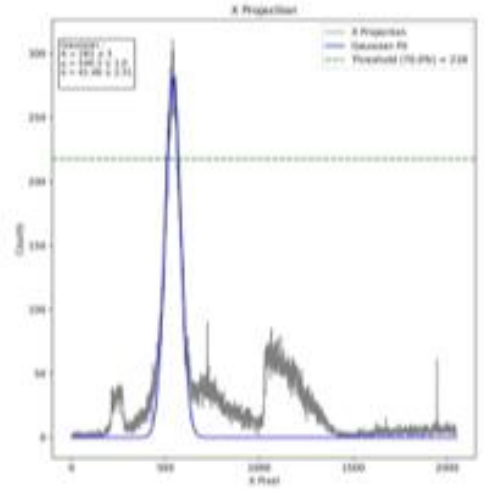

Single gaussian fit
bins >70% of peak height

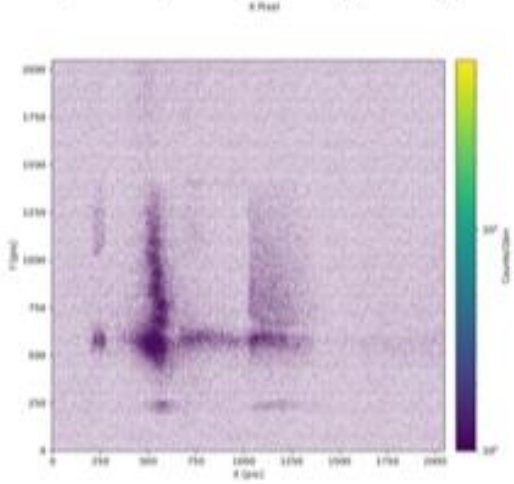

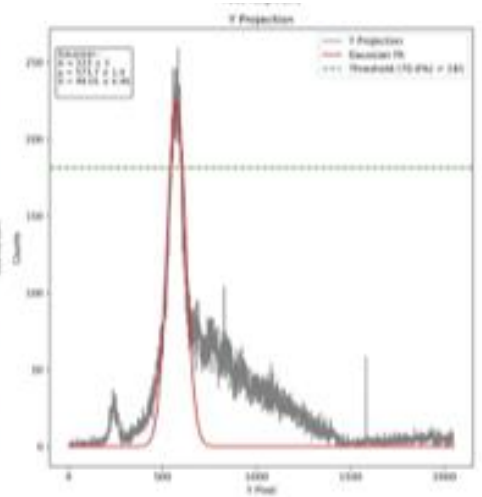

Testing Localization Accuracy

❖ Sampling points(Lookup table)

19 x 19 = **361 incident angles** and position on the detector

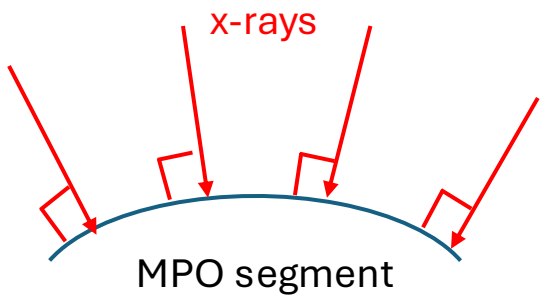

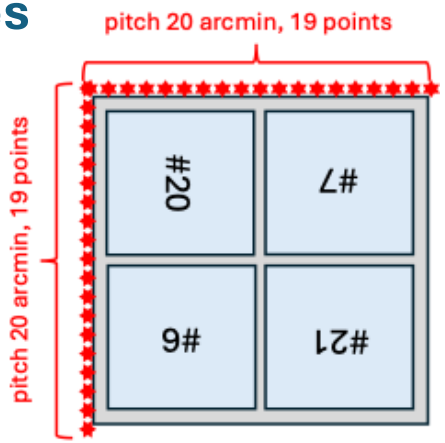

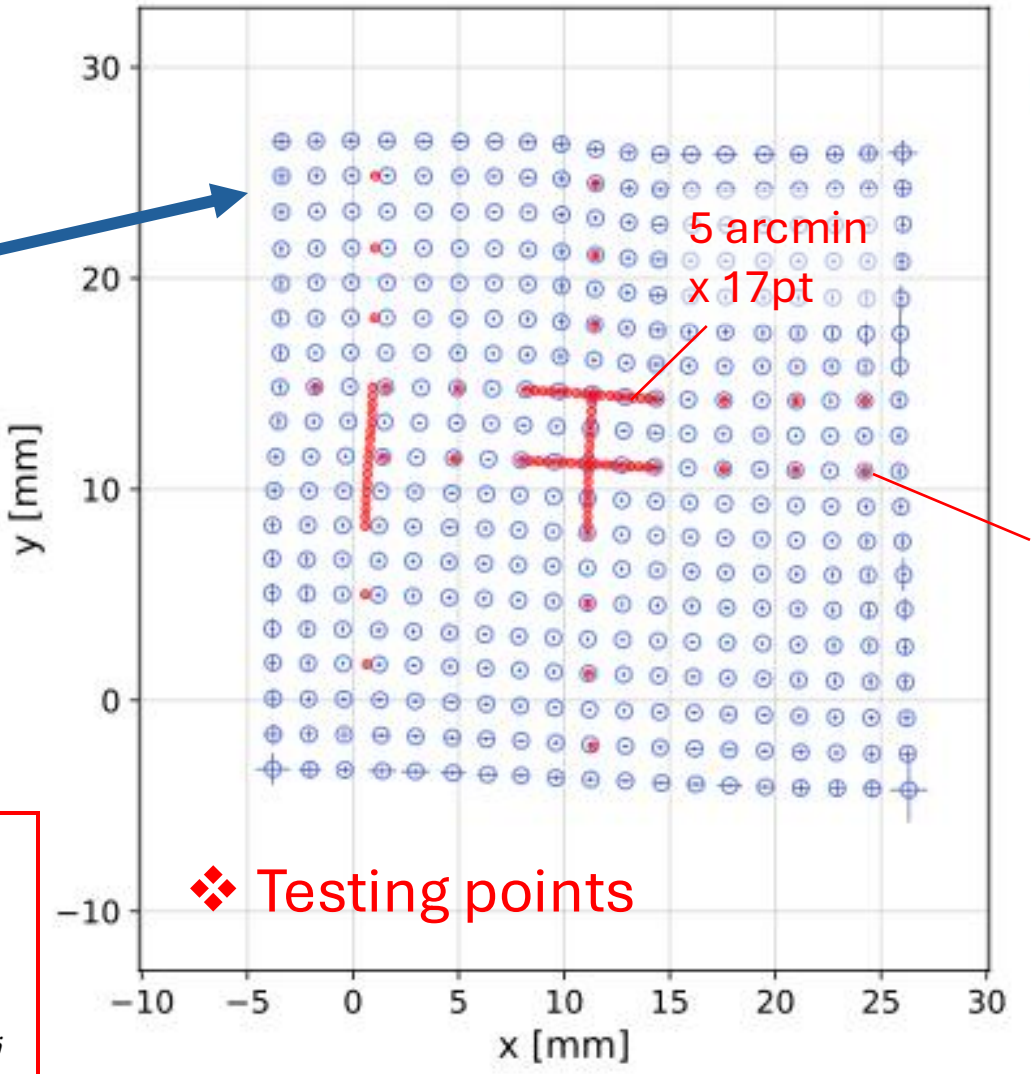

❖ Estimation of incident angle

positions $(x, y) \mapsto$ angles(θ_z, θy)

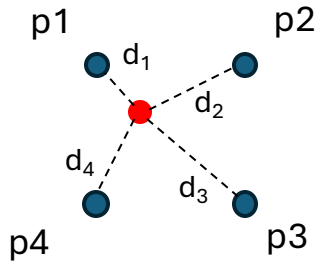

testing point (x, y)

$$w_j = \frac{1/d_j}{\sum_k 1/d_k}, \quad (k = 1\text{–}4),$$

$$\hat{\theta}_z = \sum_j w_j \, \theta_{z,j}, \qquad \hat{\theta}_y = \sum_j w_j \, \theta_{y,j}$$

weighted average

Testing Localization Accuracy

❖ [estimated angles $(x, y) \mapsto (\theta_{z\_est}, \theta_{y\_est})$] – [incident angles $(\theta_{z\_in}, \theta_{y\_in})$]

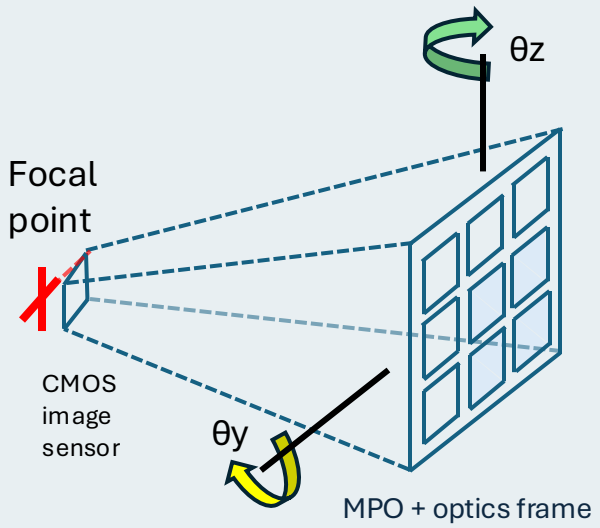

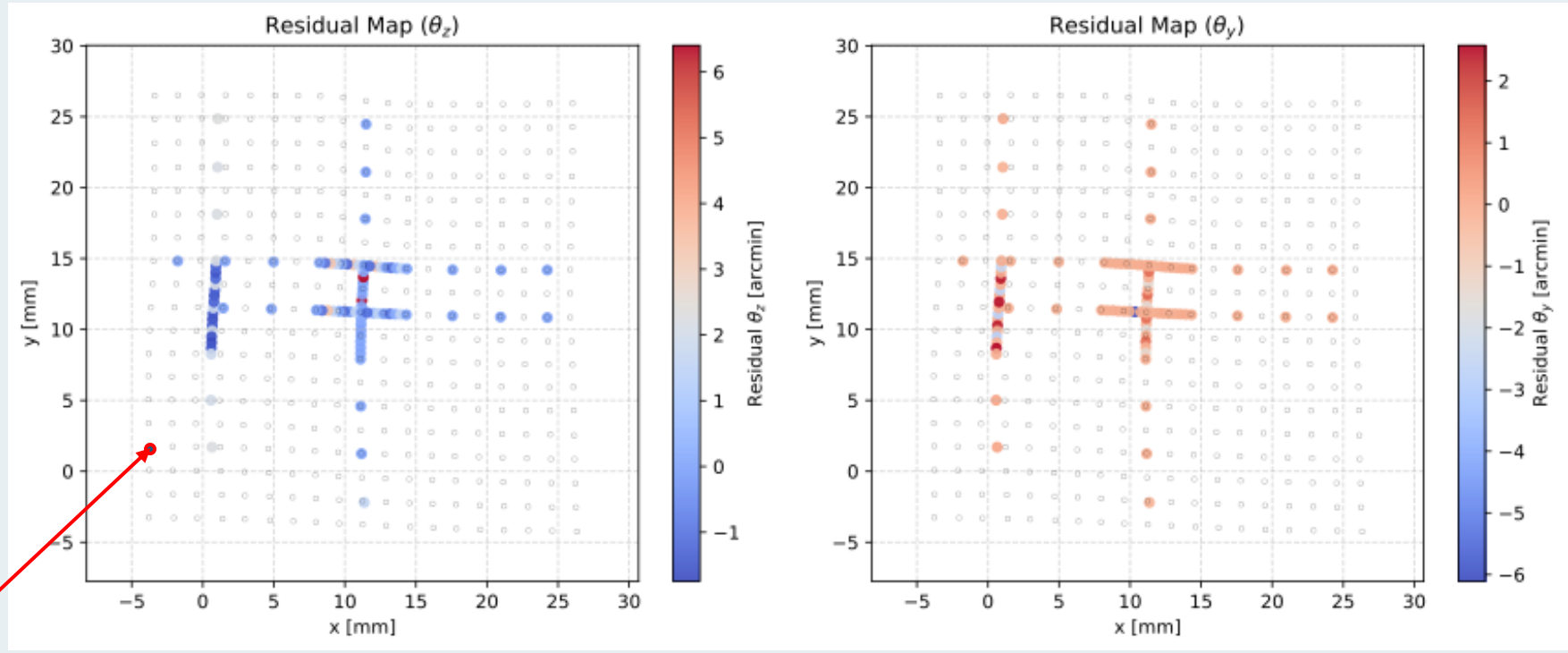

❖ Sampling points

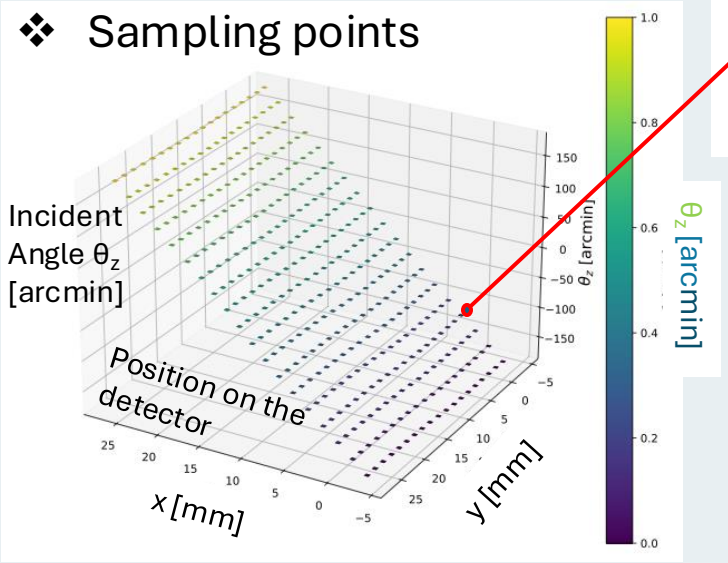

- Among 89 unique incident angles, **92.1 % angles were within ±3 arcmin error region.(< 95% = 2σ goal△)**
- Prediction of localization accuracy **with measured Point Spread Function and alignment precision** >> under the investigation

Effective Area

❖ Experimental setup

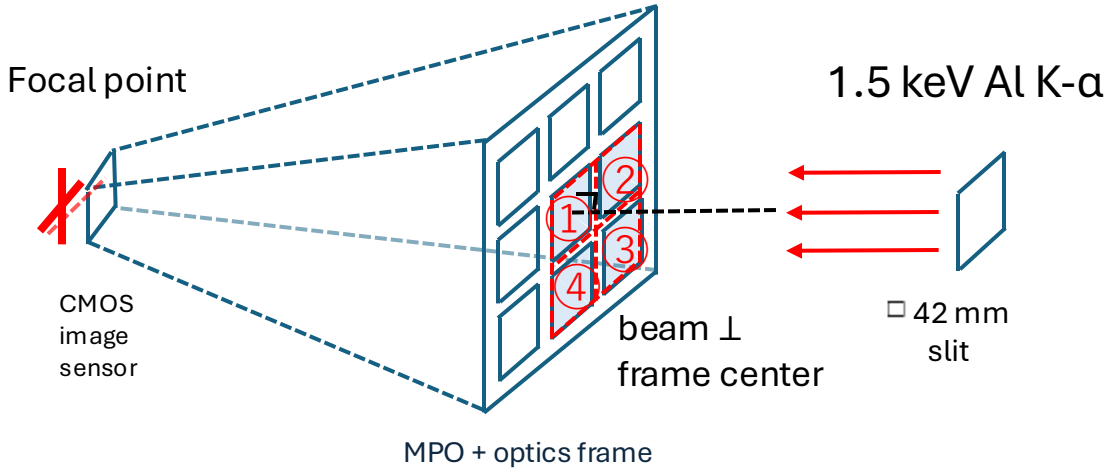

N_{focus}: focused photon count rate

N_{flux} : irradiated photon count rate in the region of $1cm^2$

Effective area ($cm^{2)}$
= N_{focus} (cts s^{-1}) ÷ N_{flux} (cts $cm^{-2}s^{-1}$)

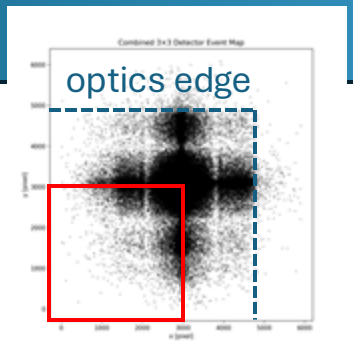

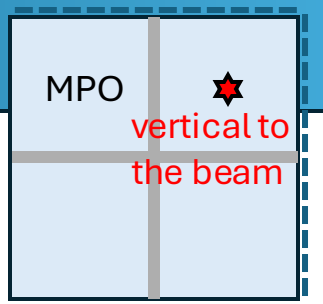

x-ray ⊙

copy & rotating third quadrant image to compensate other quadrants shape

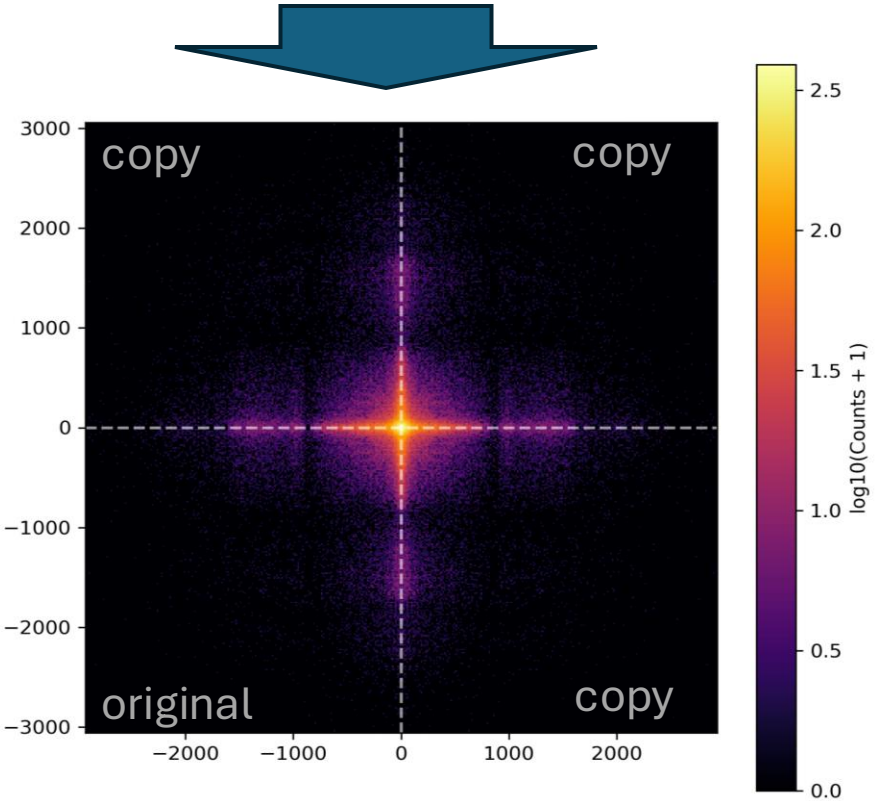

Effective Area

❖ Double gaussian fitting & obtain counts

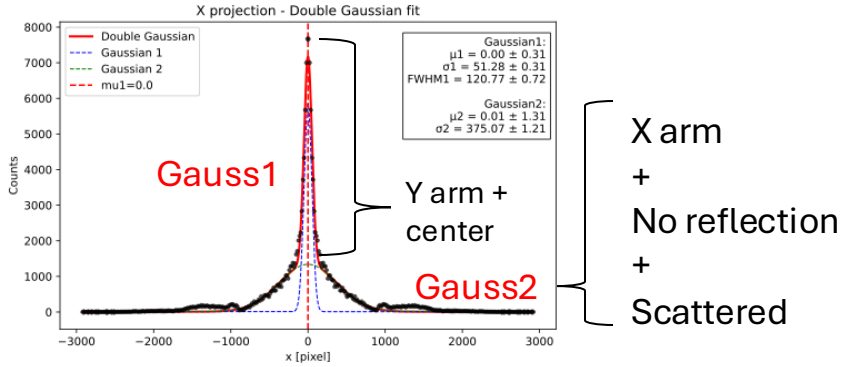

X arm
+
No reflection
+
Scattered

Y arm +
center

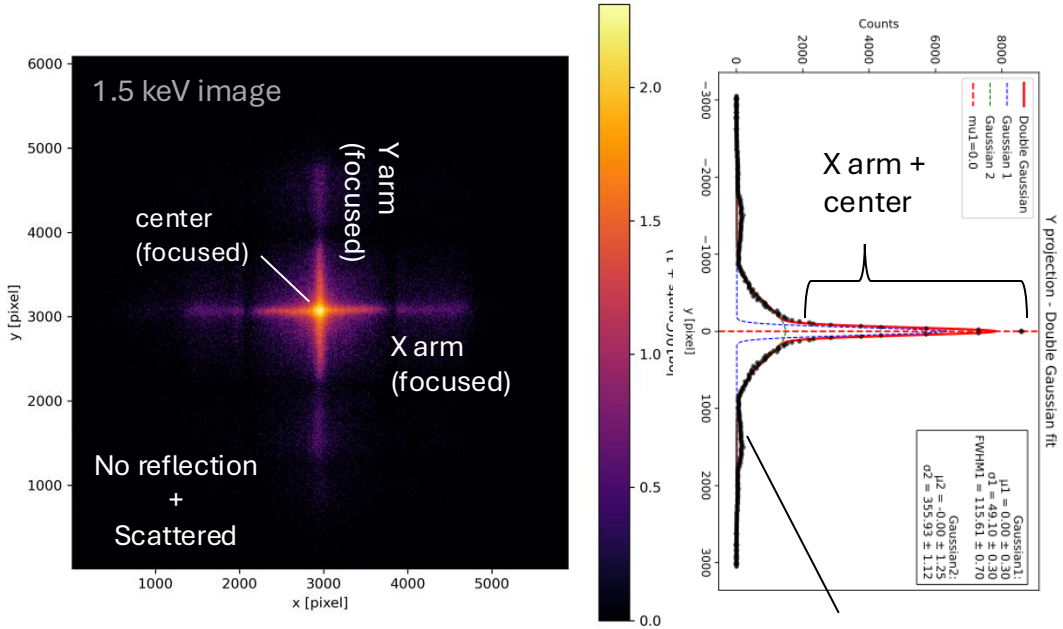

Y arm + No reflection + Scattered

❖ Effective area

by counting photons in the detector / integration of gaussian

Component	effective area [cm^2]
Total counts in the detector	**3.940 ± 0.099**
Cross (=Total counts in the detector - No reflection component)	**3.157 ± 0.082**
X arm + center	1.244 ± 0.033
Y arm + center	1.292 ± 0.034

❖Comparison with Theoretical Calculation

Uniform Optics, Considering reflectivity for each incident angle (Tamagawa et al. 2020)

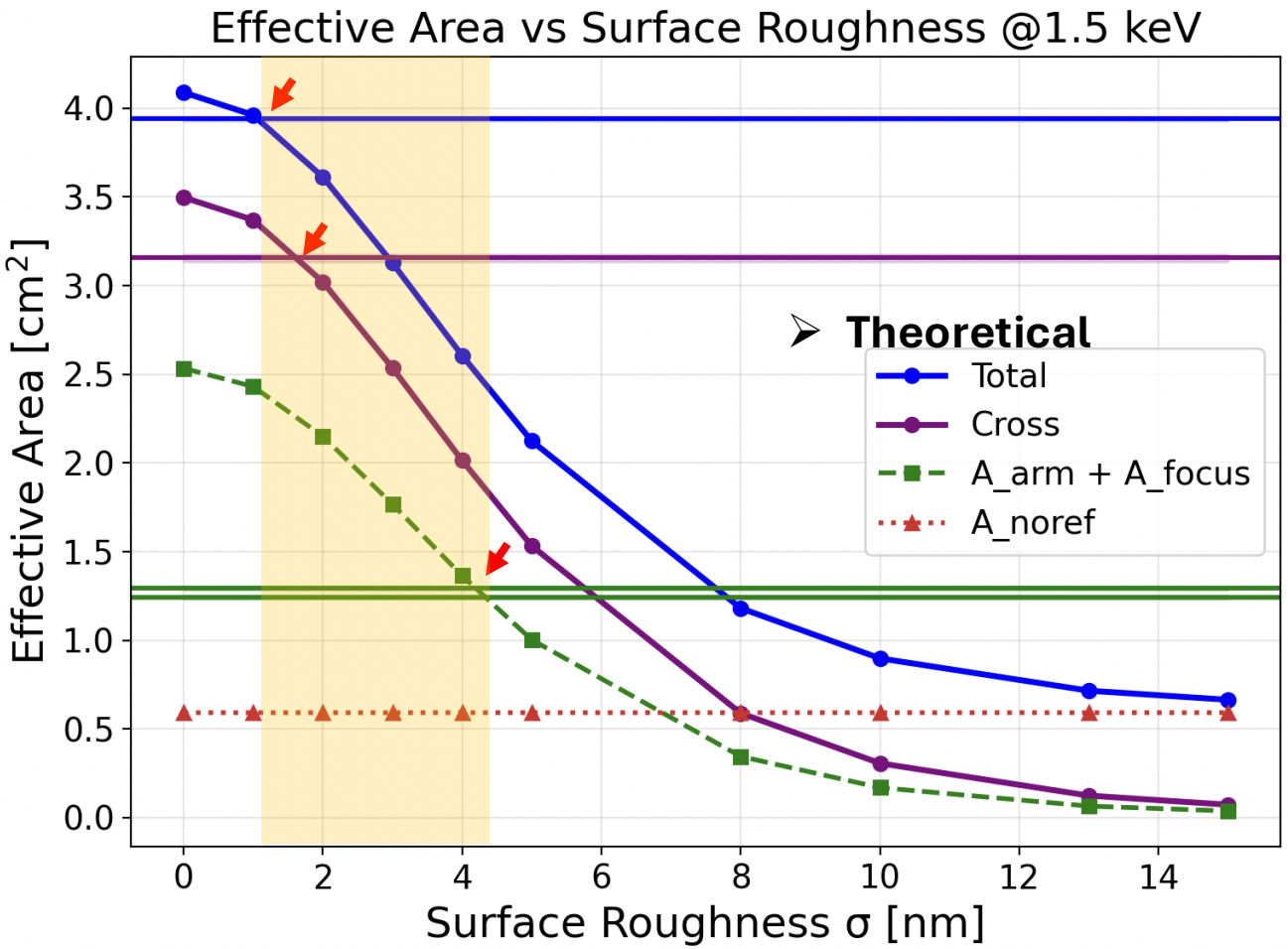

↓ Experimental (Unknown surface roughness)

Total counts in the detector

Cross

(=Total counts in the detector
- No reflection component)

X / Y axis Arm and center

- At σ = 1.1-4.3 nm, effective area of each component is consistent with the prediction.
- We are currently inquiring real surface roughness to the supplier of optics

Summary and Future Works

Summary

- ❖ We constructed and evaluated optics system prototype of EAGLE
- ❖ Achieved systematic localization accuracy of **3 arcmins with 92.1%** of tested angles
- ❖ Measured effective area:
  - **3.9403 ± 0.099 cm²** for total
  - **3.157 ± 0.082 cm²** for cross. **>Consistent with theoretical value**

Future Works

- ❖ Investigate the best methodology of incident angle estimation in limited computer resources of onboard software.
- ❖ From studying the relation of localization accuracy and MPO performance, we **set clear criteria on the best segment selection**

>> make localization accuracy of **3 arcmins 92.1% → 95 %(2σ)**

Appendix

❖ Beam stability (X-ray generator: 5 kV, 10mA)

100ms x 250 frame @reference CMOS

standard deviation: 2.34%

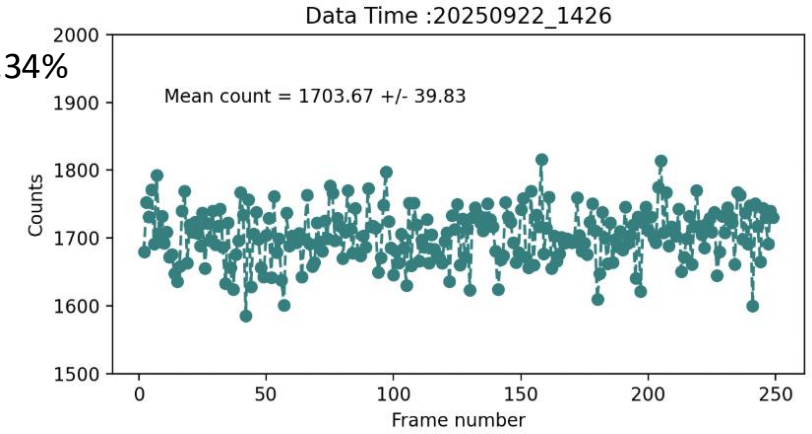

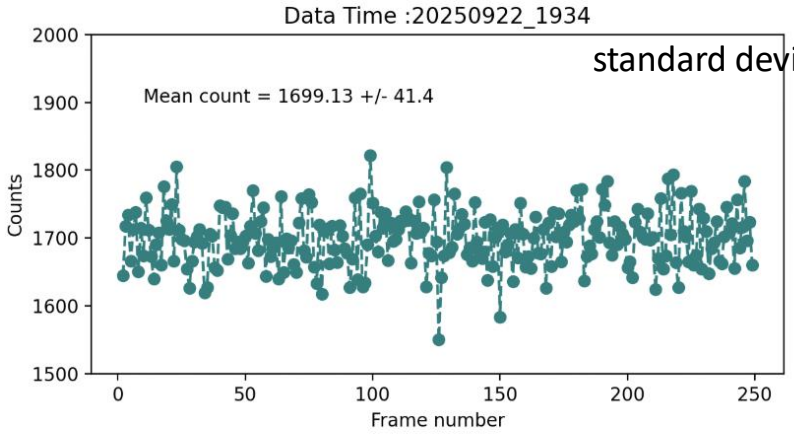

standard deviation: 2.44%

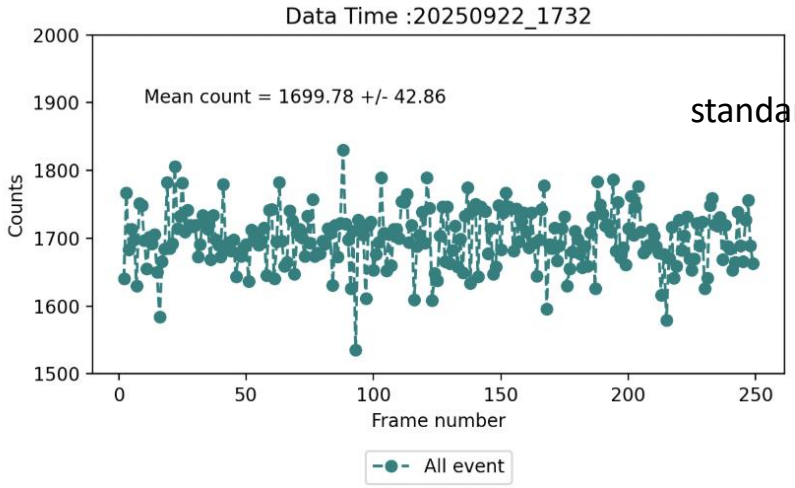

standard deviation: 2.52%

❖X-ray spectrum

Target: Al 1.5 keV
X-ray generator: 5 kV, 10mA

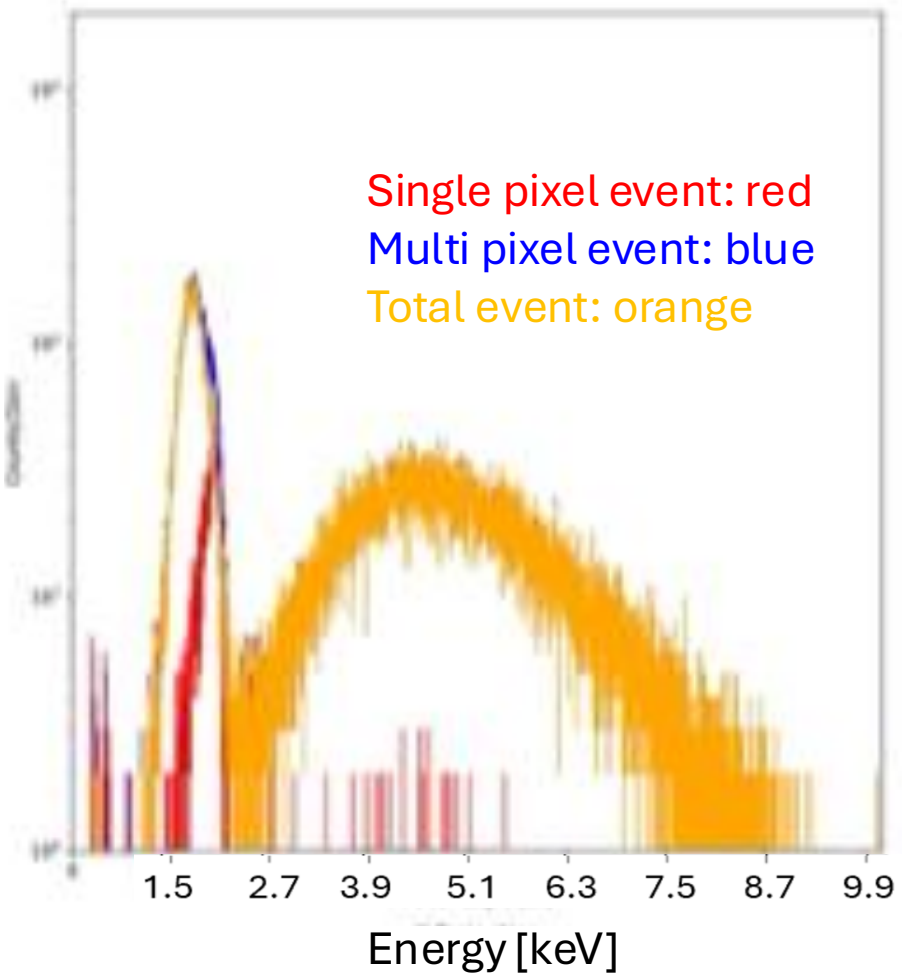

❖ Tamagawa et al. 2020

➢ Effective area of each component

$$A_{\mathrm{NoRef}}(\Theta_x,\Theta_y) = \frac{A\eta}{N^xN^y}\int_{\theta_x^{\min}}^{\theta_x^{\max}} f_0^x d\theta_x \int_{\theta_y^{\min}}^{\theta_y^{\max}} f_0^y d\theta_y$$

$$A_{\mathrm{ArmX}}(E,\Theta_x,\Theta_y) = \frac{A\eta}{N^xN^y}\int_{\theta_x^{\max}}^{\theta_x^{\min}} f_0^x d\theta_x \int_{\theta_y^{\max}}^{\theta_y^{\min}} \xi(E,\theta_y) f_1^y d\theta_y$$

$$A_{\mathrm{ArmY}}(E,\Theta_x,\Theta_y) = \frac{A\eta}{N^xN^y}\int_{\theta_x^{\min}}^{\theta_x^{\max}} \xi(E,\theta_x) f_1^x d\theta_x \int_{\theta_y^{\max}}^{\theta_y^{\min}} f_0^y d\theta_y$$

$$A_{\mathrm{Focus}}(E,\Theta_x,\Theta_y) = \frac{A\eta}{N^xN^y}\int_{\theta_x^{\max}}^{\theta_x^{\min}} \xi(E,\theta_x) f_1^x d\theta_x \int_{\theta_y^{\max}}^{\theta_y^{\min}} \xi(E,\theta_y) f_1^y d\theta_y$$

A: size of pores
η: open fraction of pores
N: number of pores
ξ: reflectivity

➢ geometrical fraction f:

- no reflection

$$f_0^i(\theta_j) = \begin{cases} 1 - \frac{\ell}{w}\tan(\theta_j) & \theta_j \le \tan^{-1}(\frac{w}{\ell}) \\ 0 & \theta_j > \tan^{-1}(\frac{w}{\ell}) \end{cases}$$

- single reflection

$$f_1^j(\theta_j) = \begin{cases} \frac{\ell}{w}\tan(\theta_j) & \theta_j \le \tan^{-1}(\frac{w}{\ell}) \\ 2 - \frac{\ell}{w}\tan(\theta_j) & \tan^{-1}(\frac{w}{\ell}) < \theta_j \le \tan^{-1}(\frac{2w}{\ell}) \\ 0 & \theta_j > \tan^{-1}(\frac{2w}{\ell}) \end{cases}$$

l: thickness of MPO
w: width of micro pores

❖ Effective area in other GRB Lobster X-ray monitor

➢ WXT/Einstein Probe (Cheng et al. 2025)

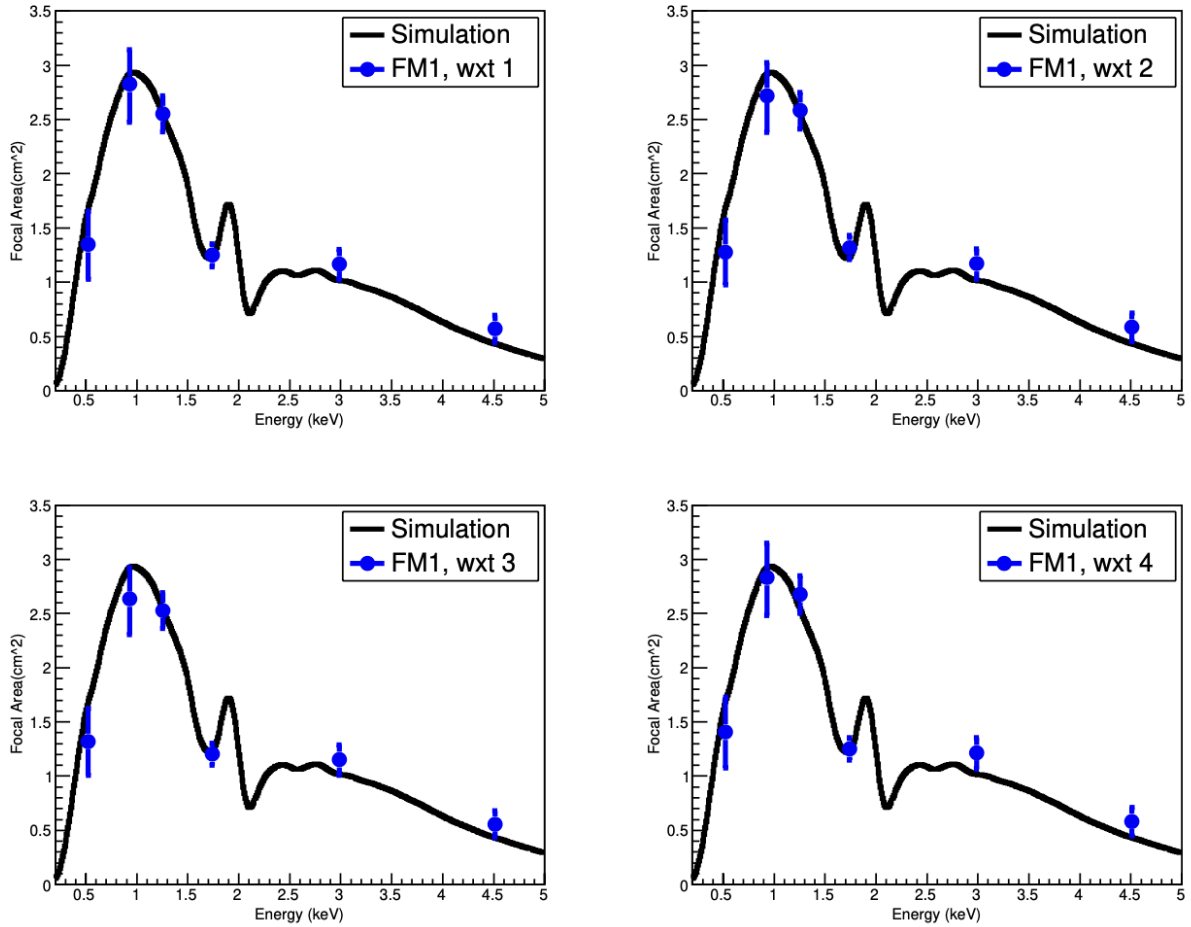

Fig. 9 The effective area as a function of the energy of incident photons, measured in the direction along the center of the four CMOS detectors aboard FM1 (CMOS 1-4). The blue dots are the measurements at different energies and the black solid line denotes the simulated model over-plotted for comparison.

❖Geometry and focusing component

- number of reflection at wall (nx, ny)

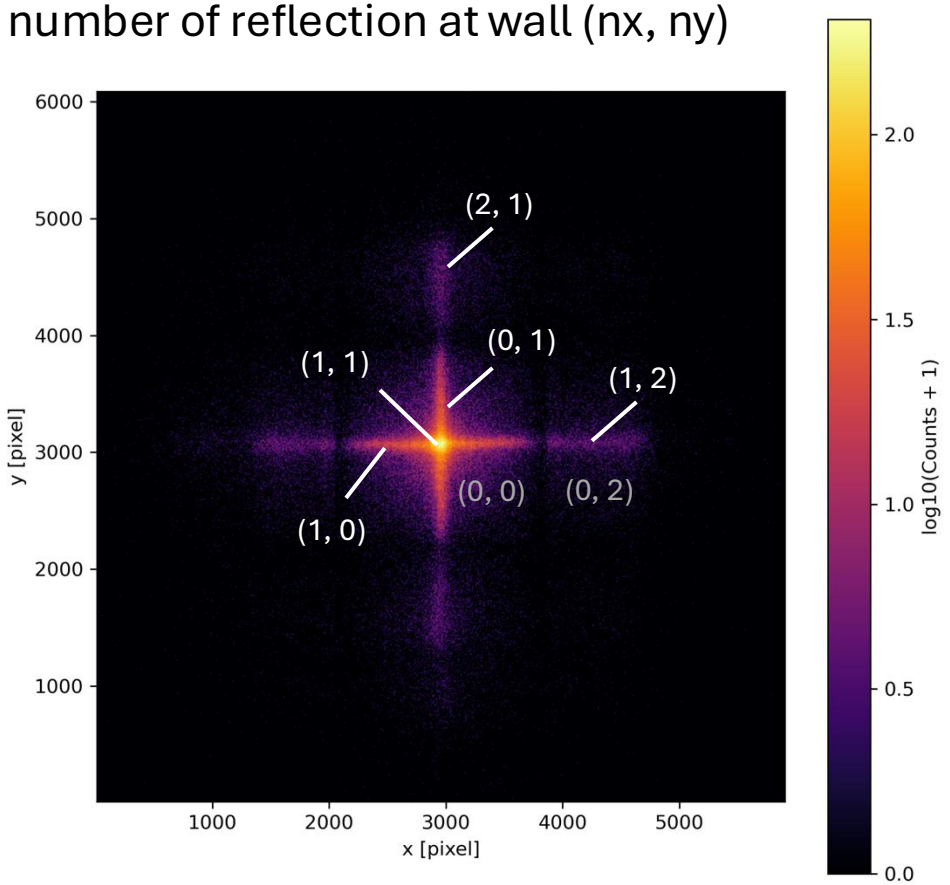

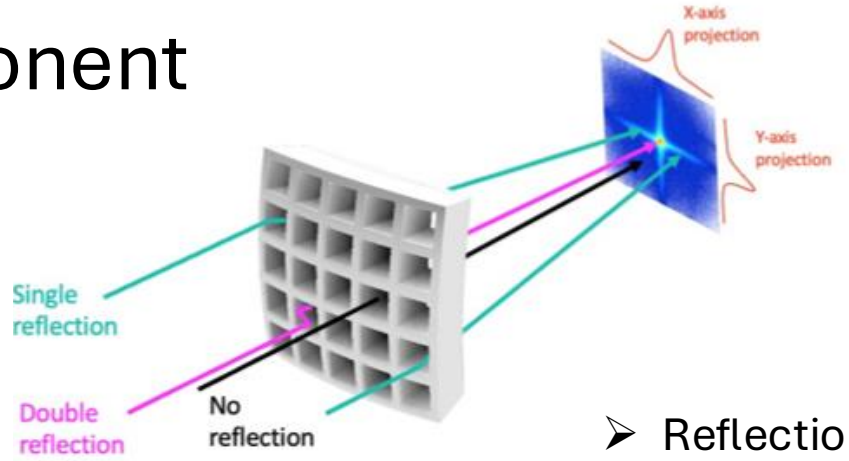

- Reflection in same x/y axis

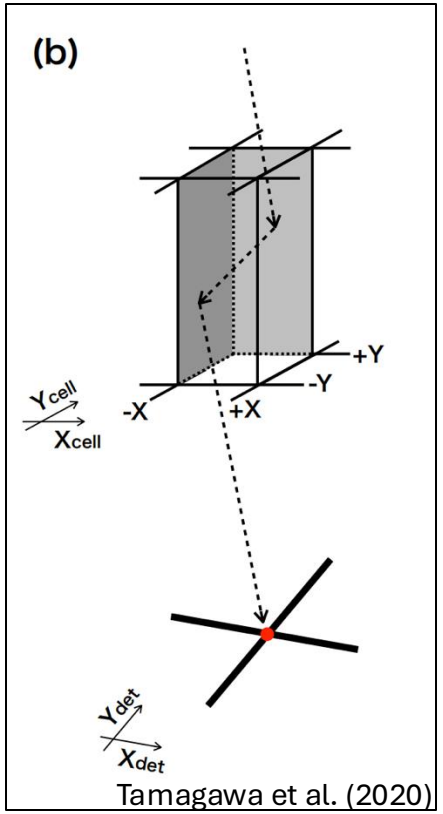

Tamagawa et al. (2020)

1 reflection

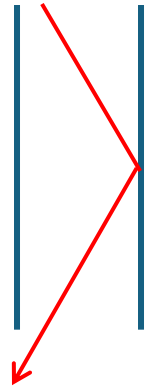

2 reflection

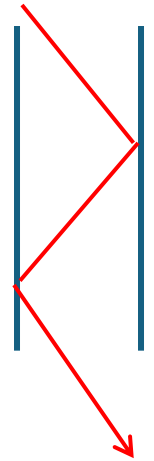

❖ Testing PSF with double gaussian and Lorentzian, single gaussian

Al 1.5 keV on-axis event map

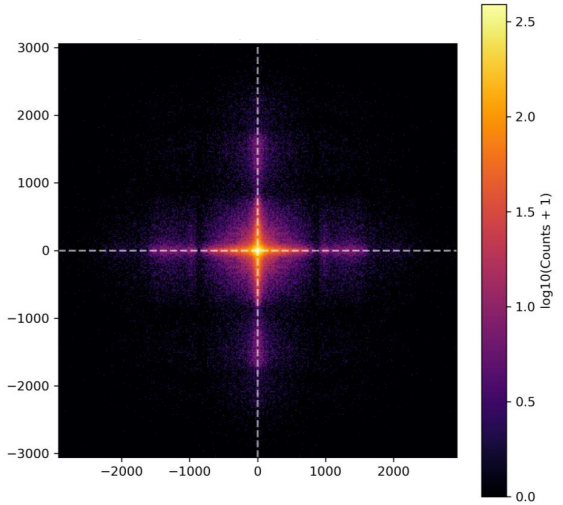

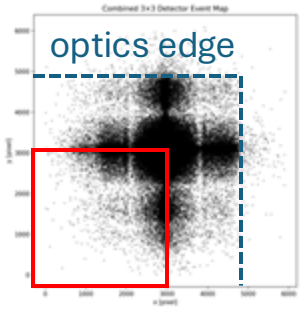

copy & rotating third quadrant image to compensate other quadrants shape

Double gaussian

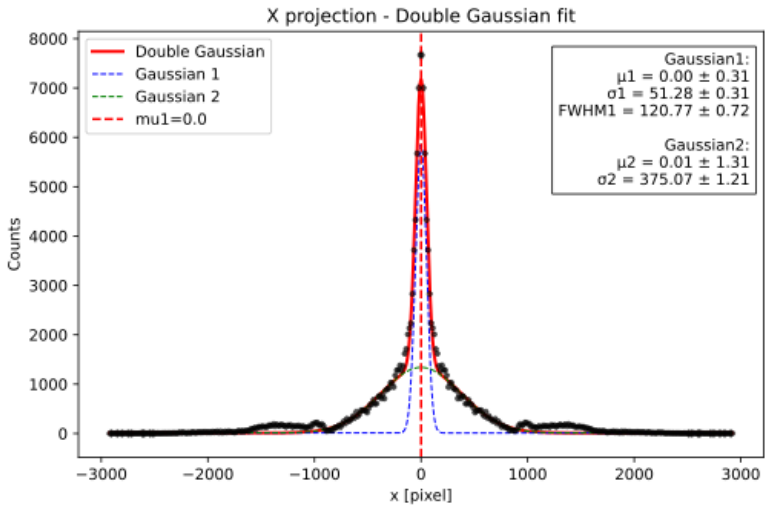

Lorentzian

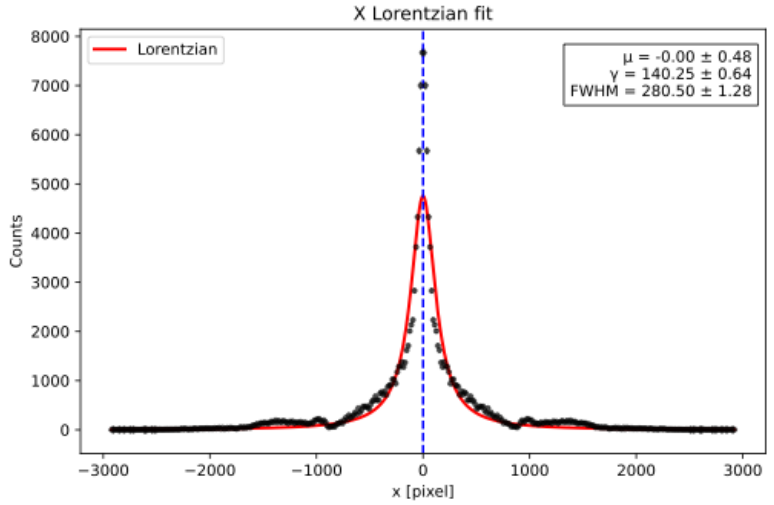

Single gaussian

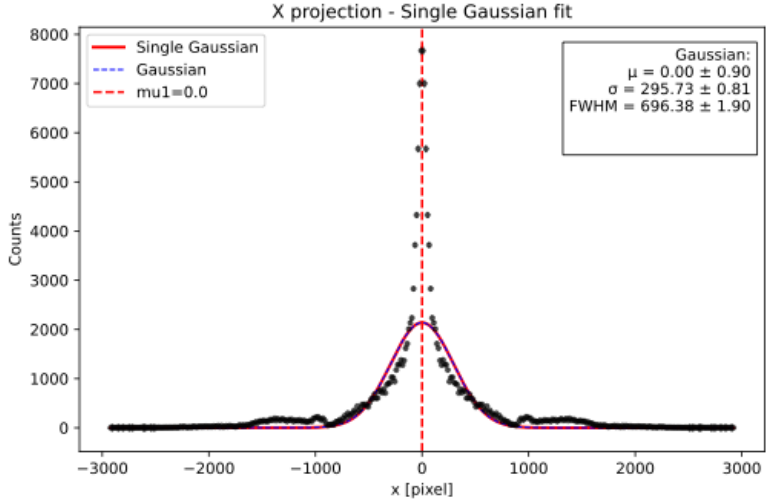

Double gaussian

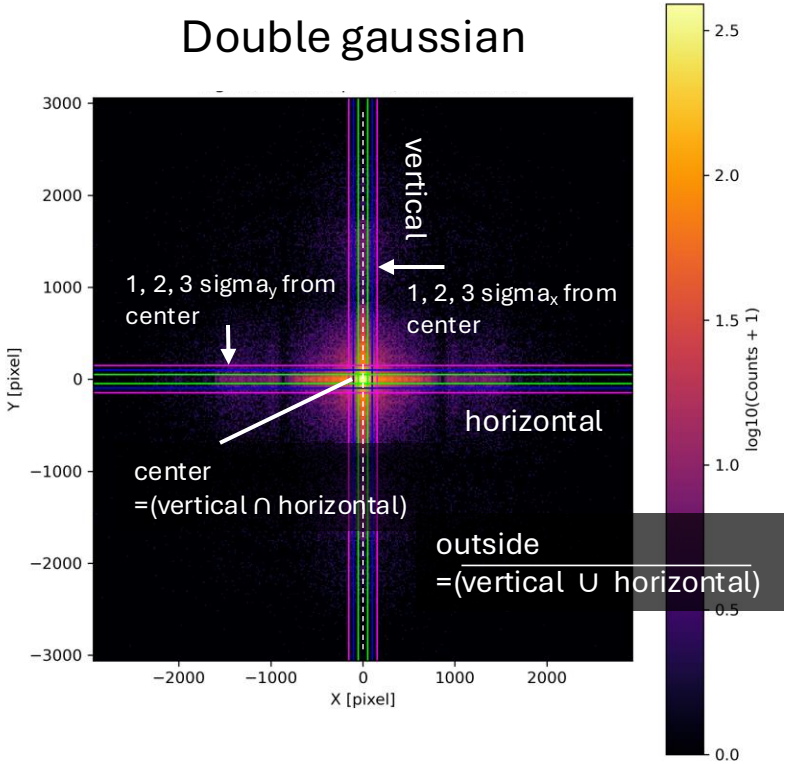

<Counts in each component for different width>

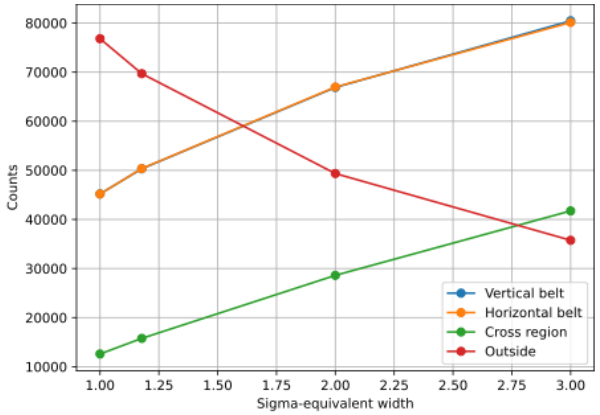

Lorentzian

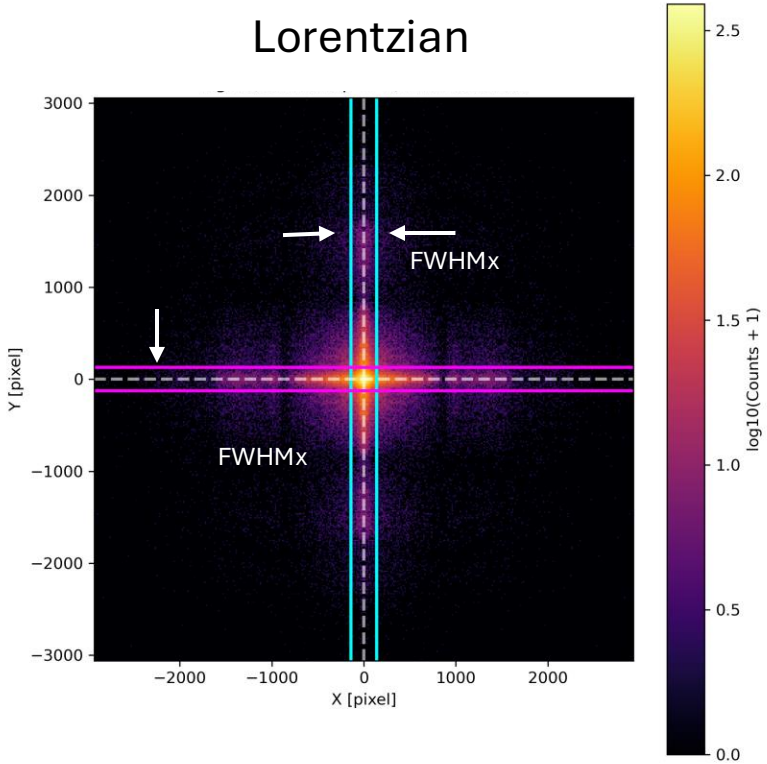

<FWHM counts>
vertical: 77128
horizontal: 75508
center: 37504
outside: 39480
cross/total ratio = 74.47 %

Single gaussian

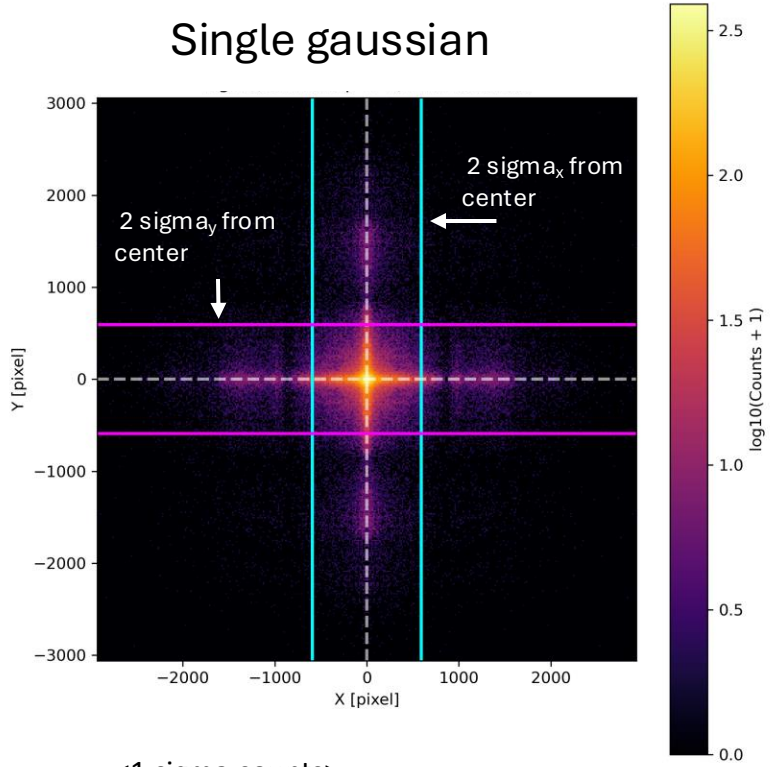

<1 sigma counts>

vertical: 103624
horizontal: 103900
center: 70344
outside: 17432
cross/total ratio = 88.73 %

<2 sigma counts>

vertical: 128984
horizontal: 128832
center: 107784
outside: 4580
cross/total ratio = 97.04 %

➢Reflectivity and incident angle

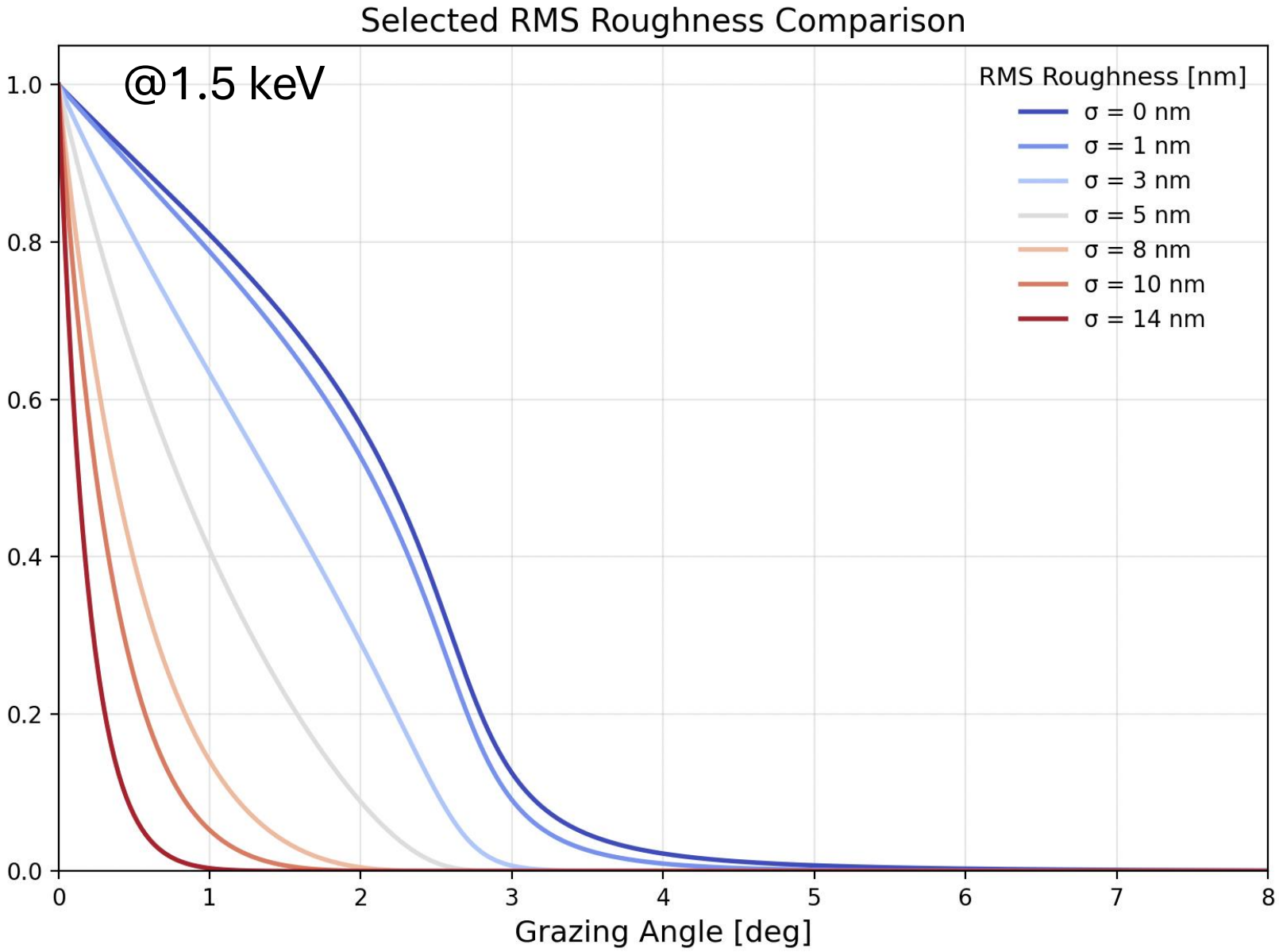

➢3x3 MPO Effective area (eq. from Tamagawa et al. 2020)

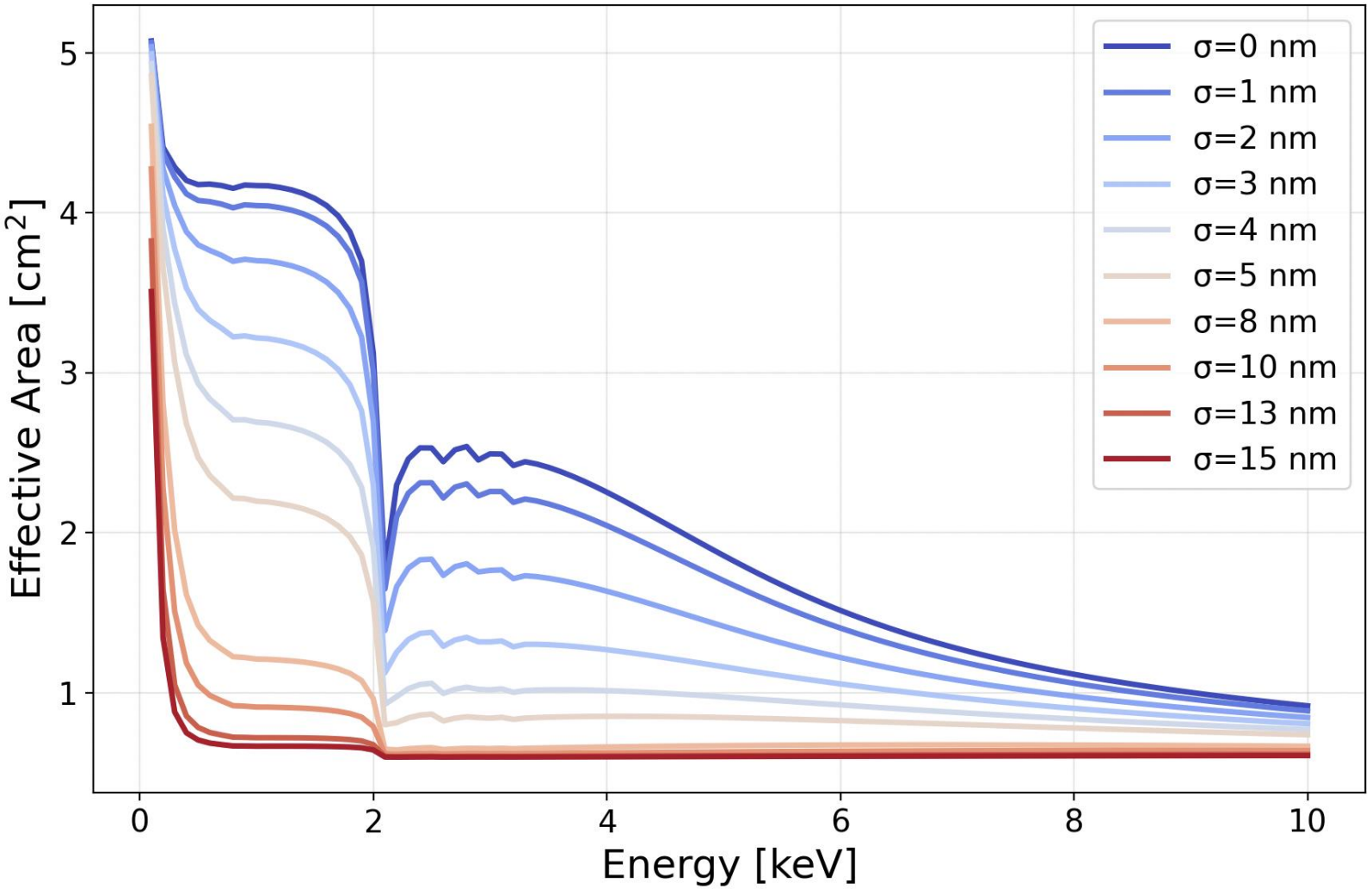

Testing Localization Accuracy

- Comparison of the actual incident angles and the estimated incident angles derived from the focal positions

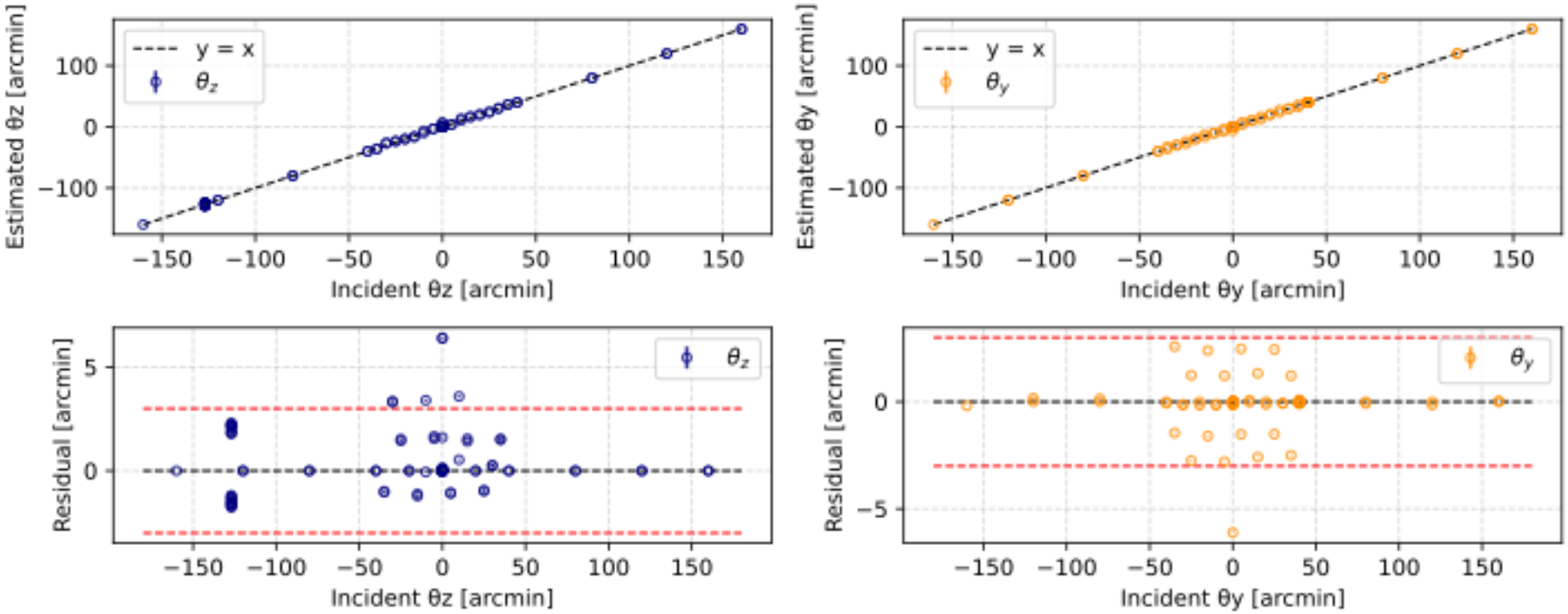

Testing Localization Accuracy

❖ [estimated angles $(x, y) \mapsto (\theta_{z\_est}, \theta y_{\_est})$] – [incident angles $(\theta_{z\_in}, \theta y_{\_in})$]

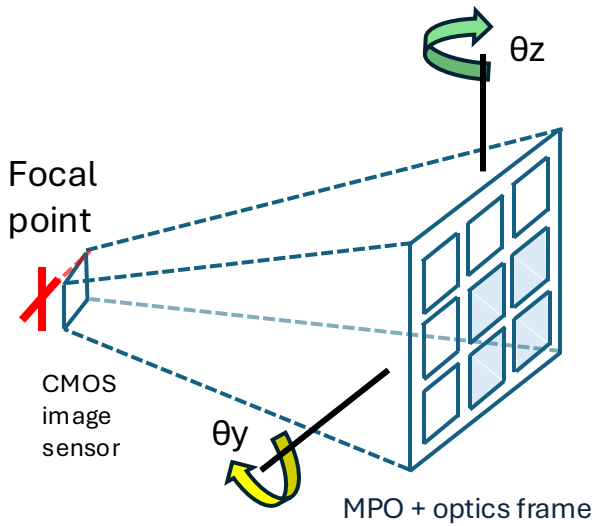

❖ Sampling points

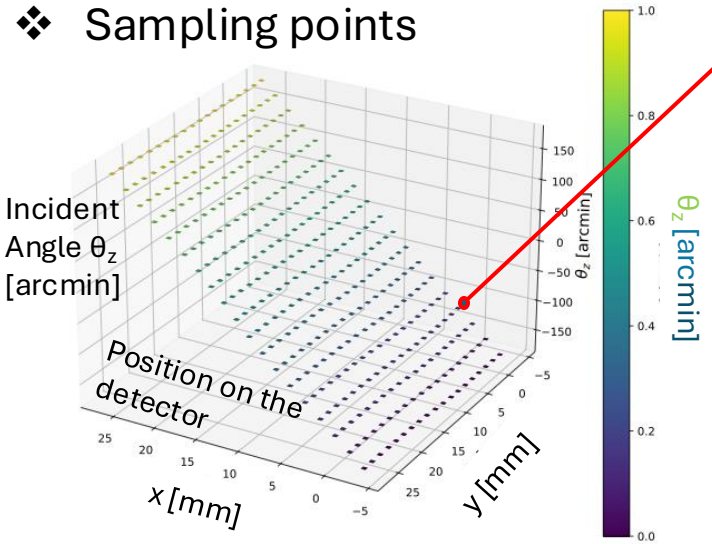

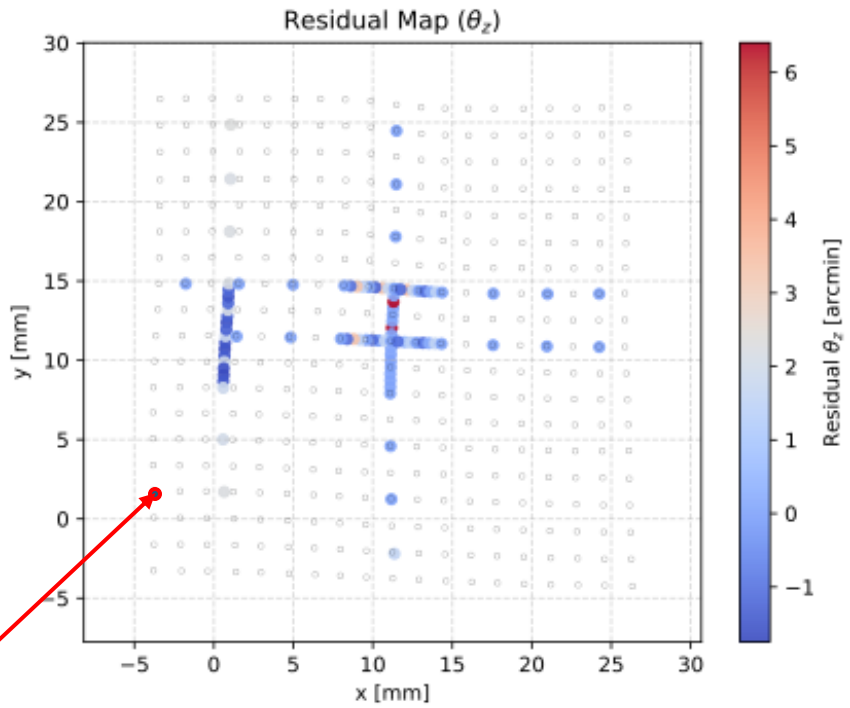

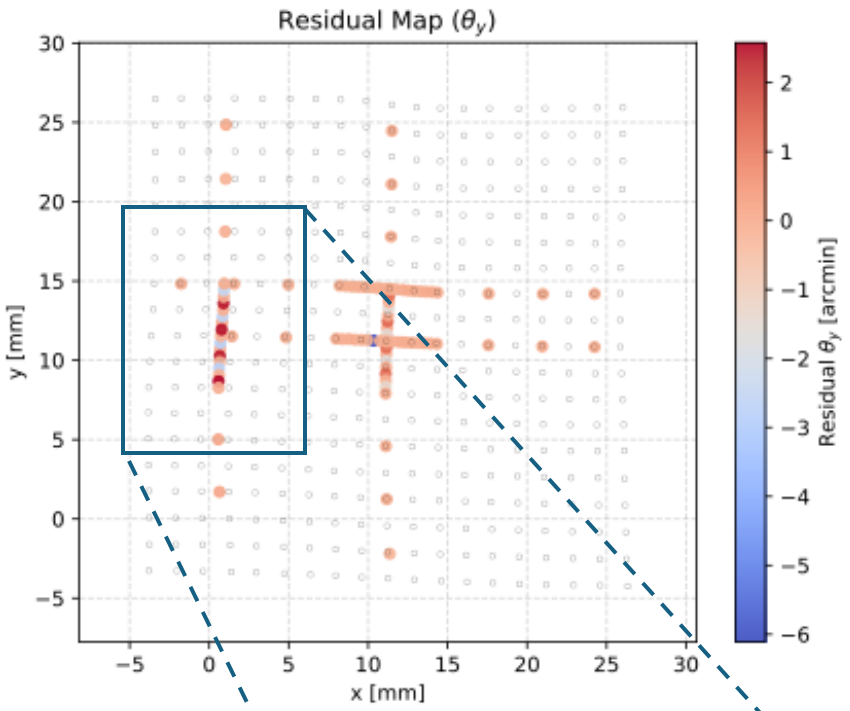

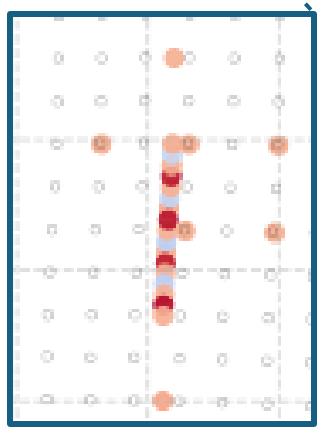

- Among 89 unique incident angles, 7 (92.1 %) incident angles were within ± 3 arcmin error region.
- To achieve 95 %(2σ) as a goal, we need further investigation in both of construction and estimation method.

❖Simulate localization accuracy for different alignment precision

Define point spread function (PSF) of a double Gaussian

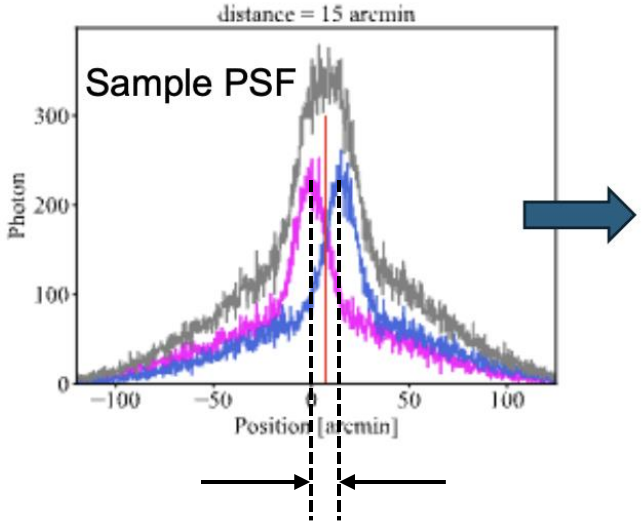

Separation angle of peak= alignment precision

10000 Monte Carlo simulations, calculate centroid of N photons

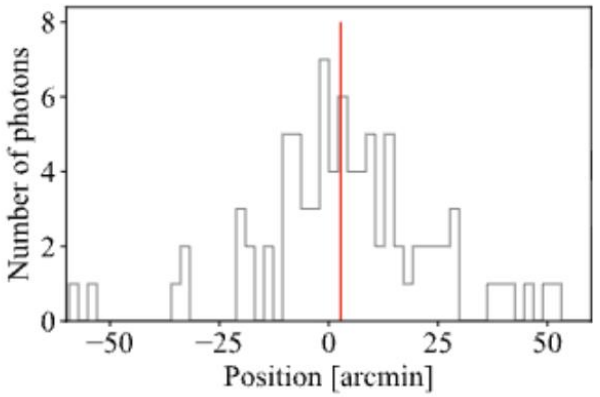

Color shows the range that contains 68% of the centroid distribution (R68) for different peak separations and photon counts

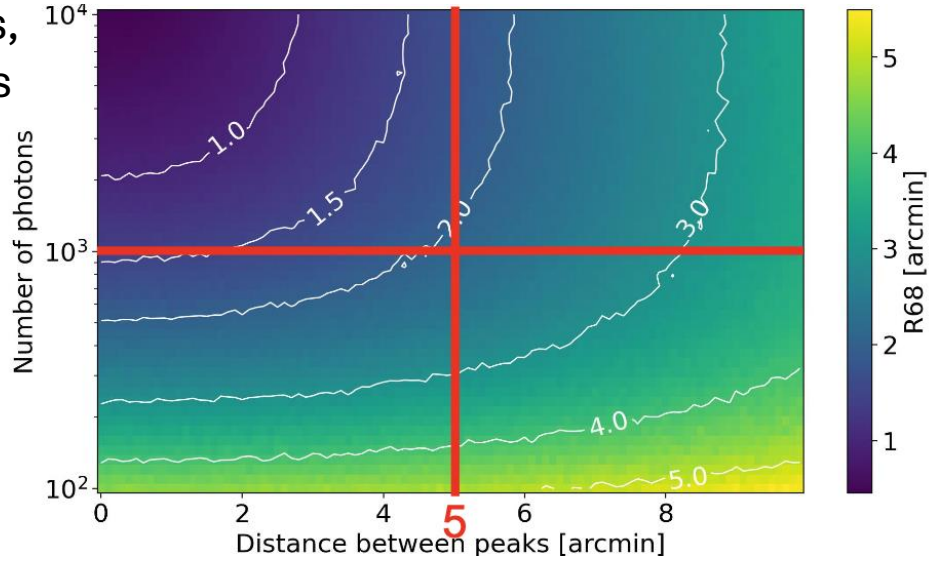

❖Quadrant extrapolation of Event Map

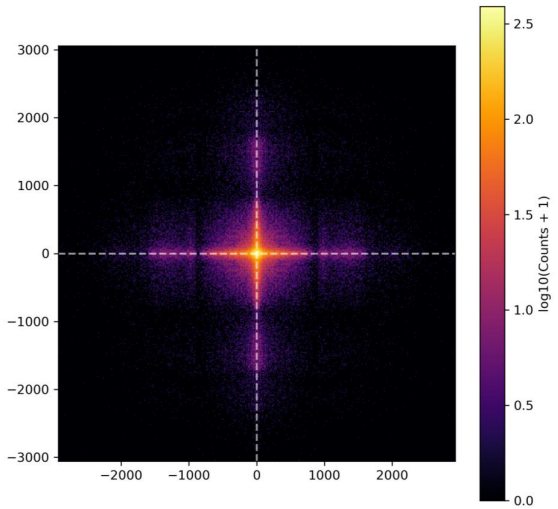

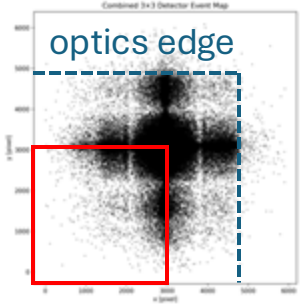

copy & rotating third quadrant image to compensate other quadrants shape

- A single Gaussian fit to the XY projection of the event map to find the boundary of quadrants.

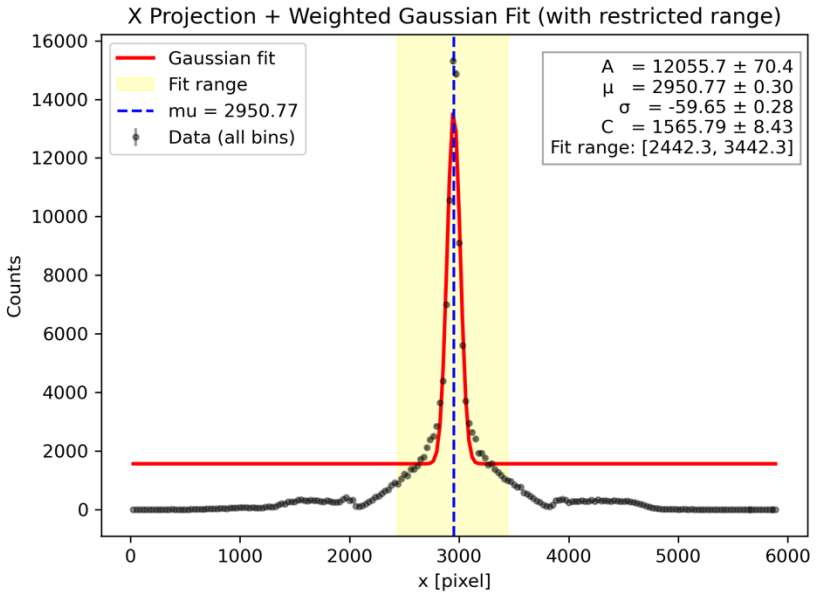

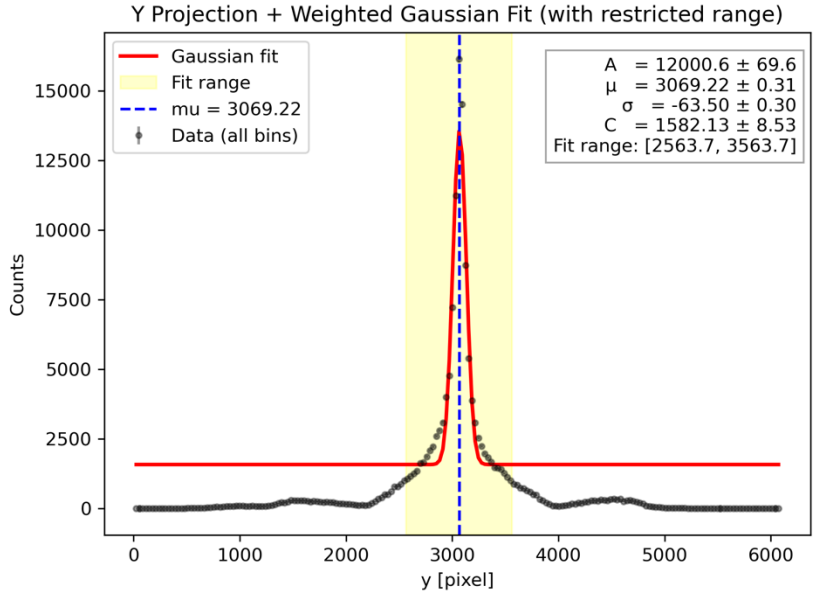

Alignment with X-ray measurement (2023)

Kanazawa University 5 m X-ray beamline
+Thermal vacuum chamber (10^{-3} Pa)

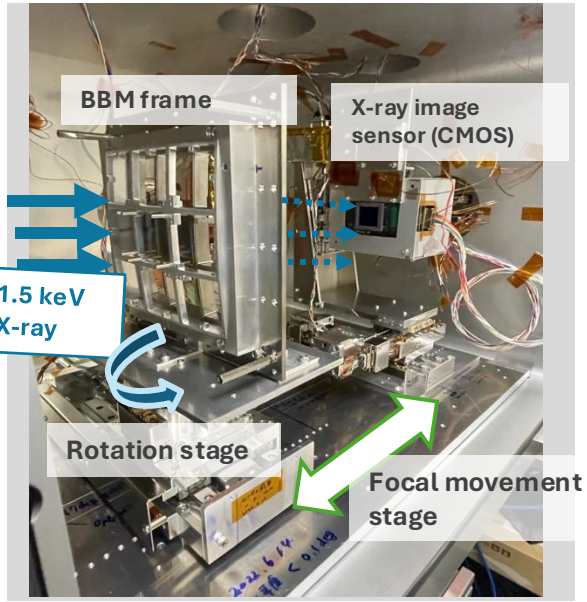

(1) 1st X-ray measurement

X-ray focused image from two LEOs

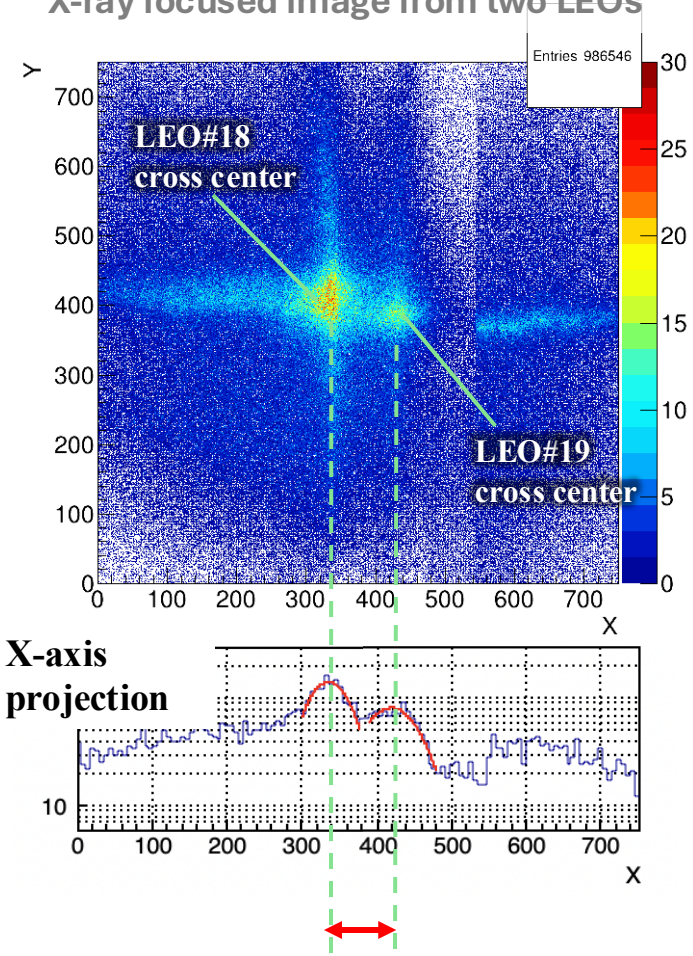

Distance of cross center
dθx : 24.6 arcmin
dθy : 5.4 arcmin

(2) Adjustment

x shim: +0.12 mm
y shim: -0.03 mm

(3) 2nd X-ray measurement

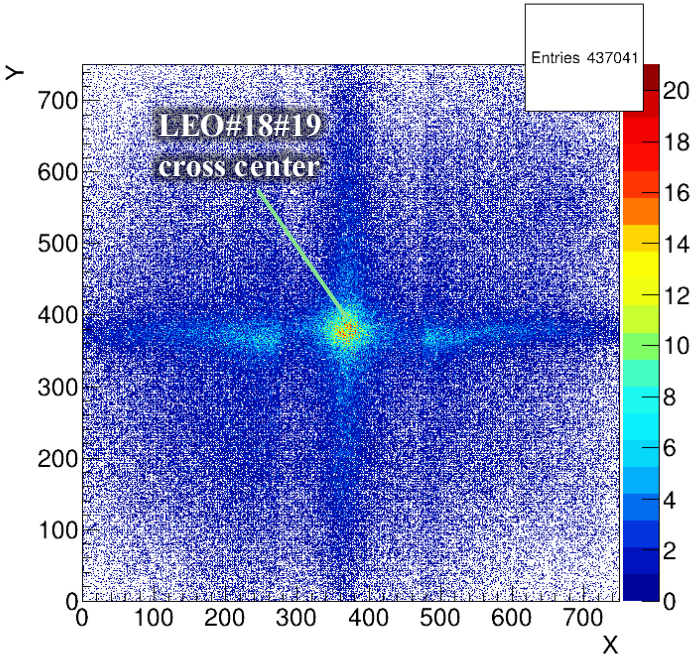

axis	Distance between two cross center
X	2.67+/- 0.09 arcmin **<<10 arcmin**
Y	1.34 +/- 0.53 arcmin **<< 10 arcmin**

We can catch the transient in NIRT at 99 % probability

Focal Length

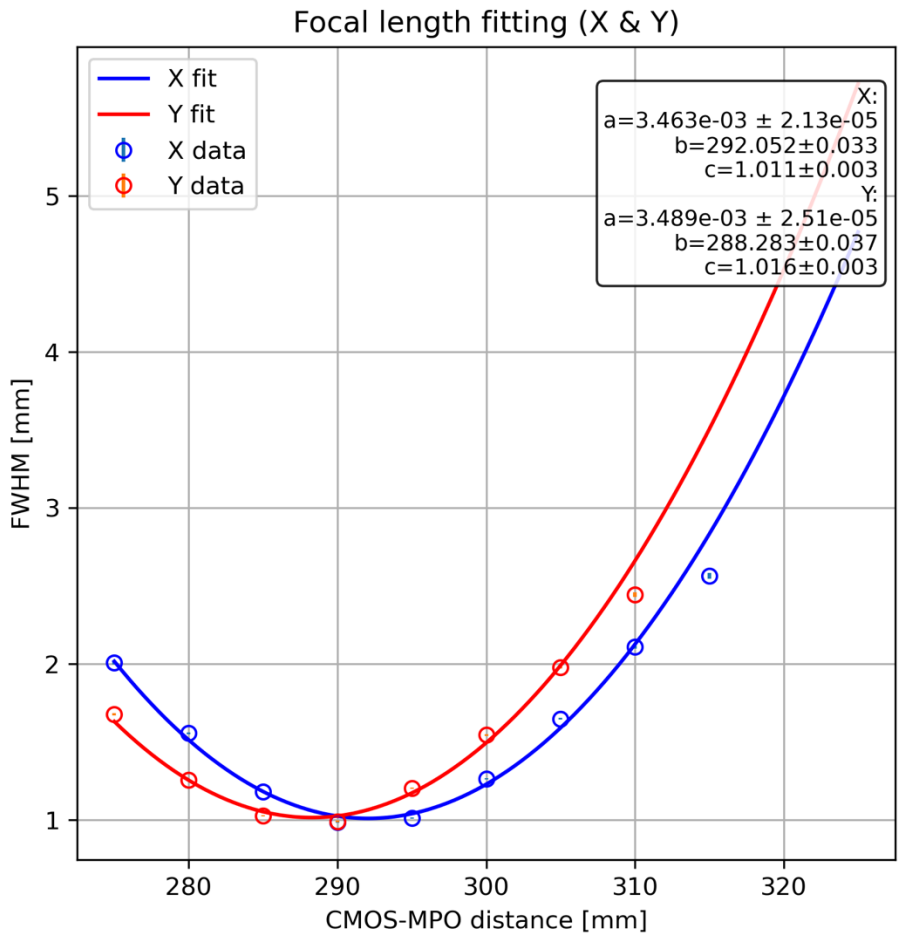

➢ Focal length for each MPO segments

MPO ID	X [mm]	Y [mm]
#19	300.47	294.32
#4	282.51	285.95
#21	289.39	285.66
#7	296.45	292.35
#20	295.89	291.98
#18	287.90	296.31
#6	295.98	293.19

red: selected segments

Angular Response of MPO Segments

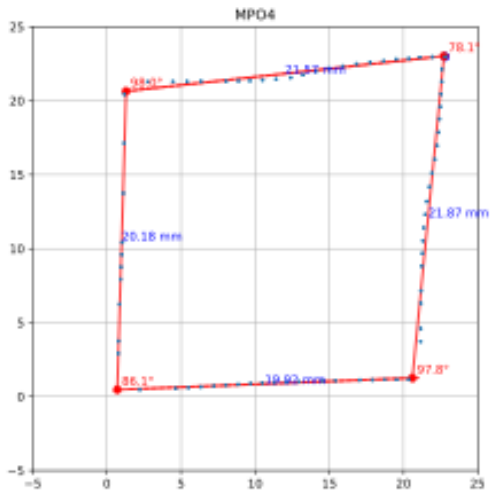

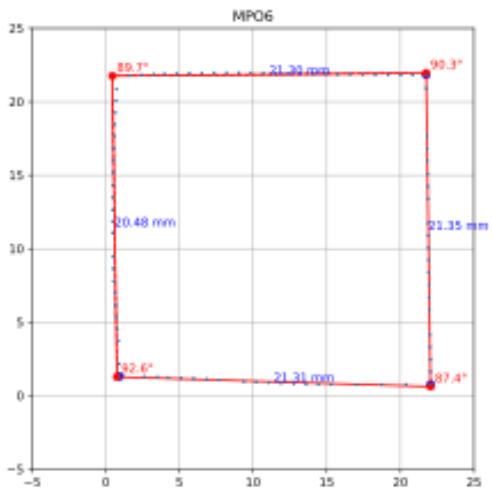

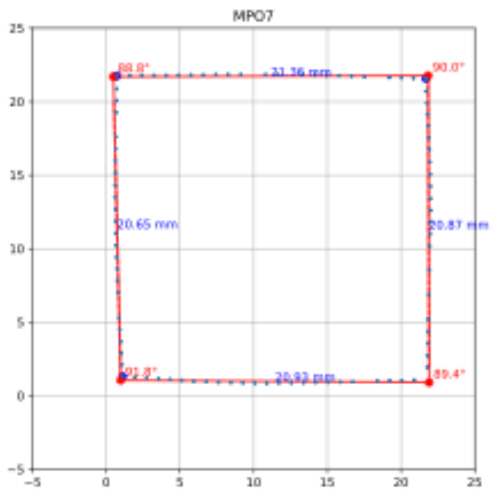

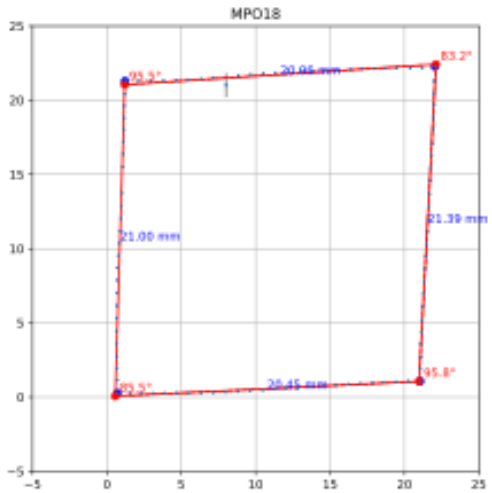

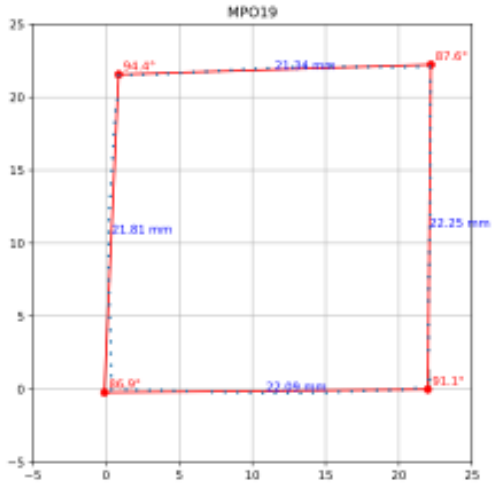

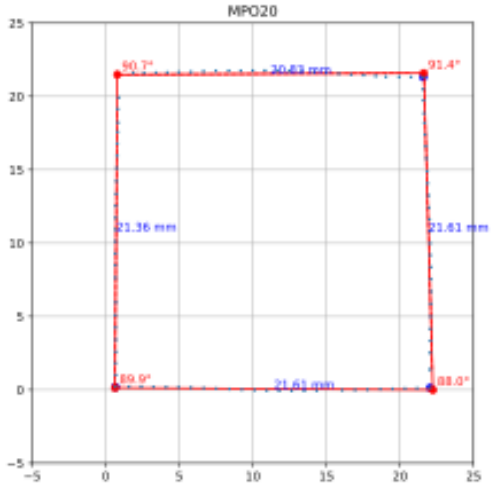

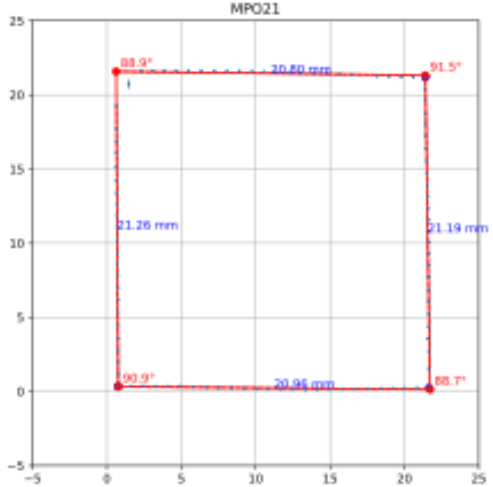

❑ Selection of MPO

データ元:　2025/8/28-29での各素子の焦点距離測定
□ 10 mmスリット 4x4グリッド

https://docs.google.com/spreadsheets/d/1zBKyehjjdrE3hXpE-yQutbOxz3lj-NY_ltJmf8KIBz4/edit?gid=452614880#gid=452614880

MPO ID	X	Y	平均 [mm]	
#19	300.47	294.32	297.39	
#4	282.51	285.95	284.23	×角度応答の歪みが大きい
#21	289.39	285.66	287.52	
#7	296.45	292.35	294.40	
#20	295.89	291.98	**293.93**	◎角度応答の形状に歪みがなく、4枚平均に最も近い >>フレーム中心の基準MPOと定める
#18	287.90	296.31	292.11	△焦点距離は平均値に近いが 角度応答の歪みが大きい
#6	295.98	293.19	294.58	

赤色: アライメント調整に用いるMPO

Angular Response

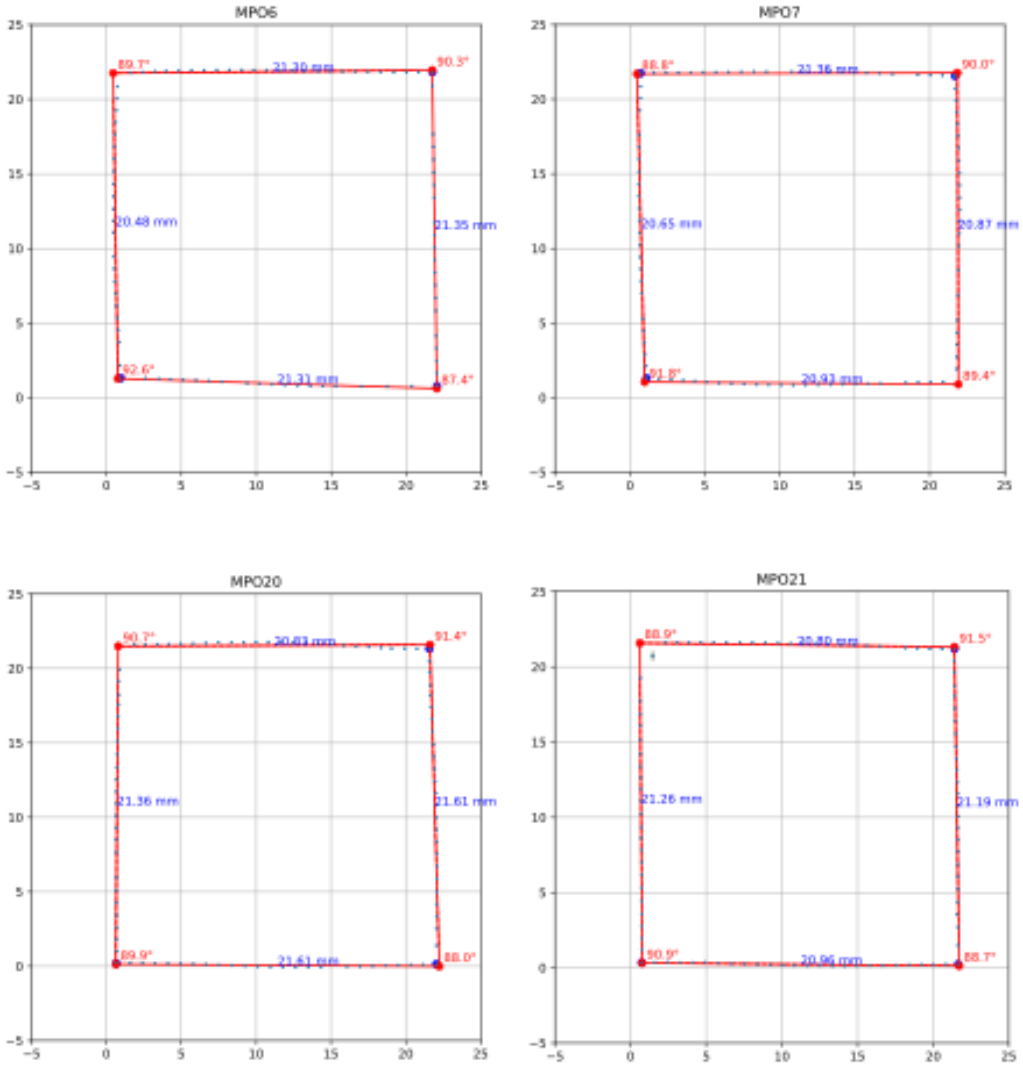

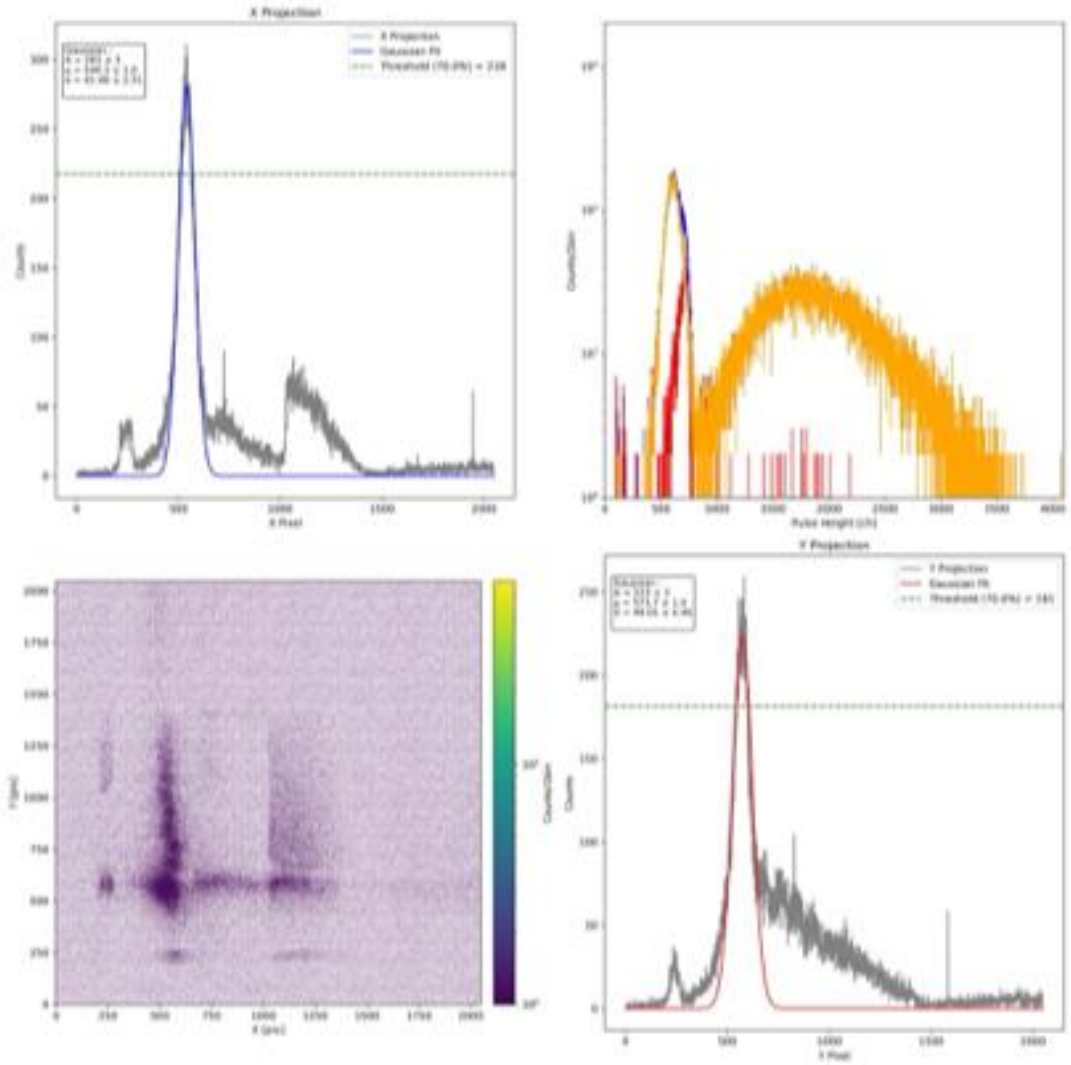

Alignment of MPO Segments

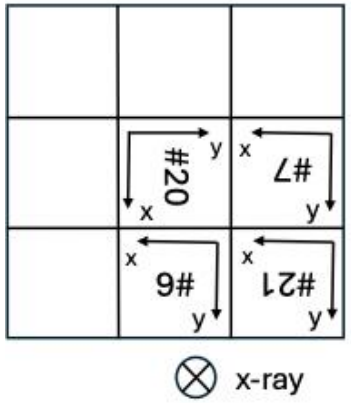

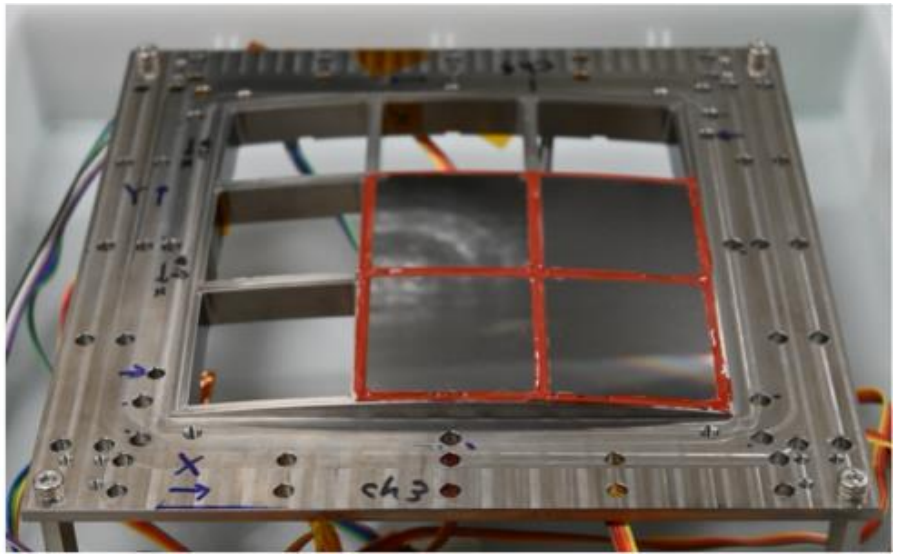

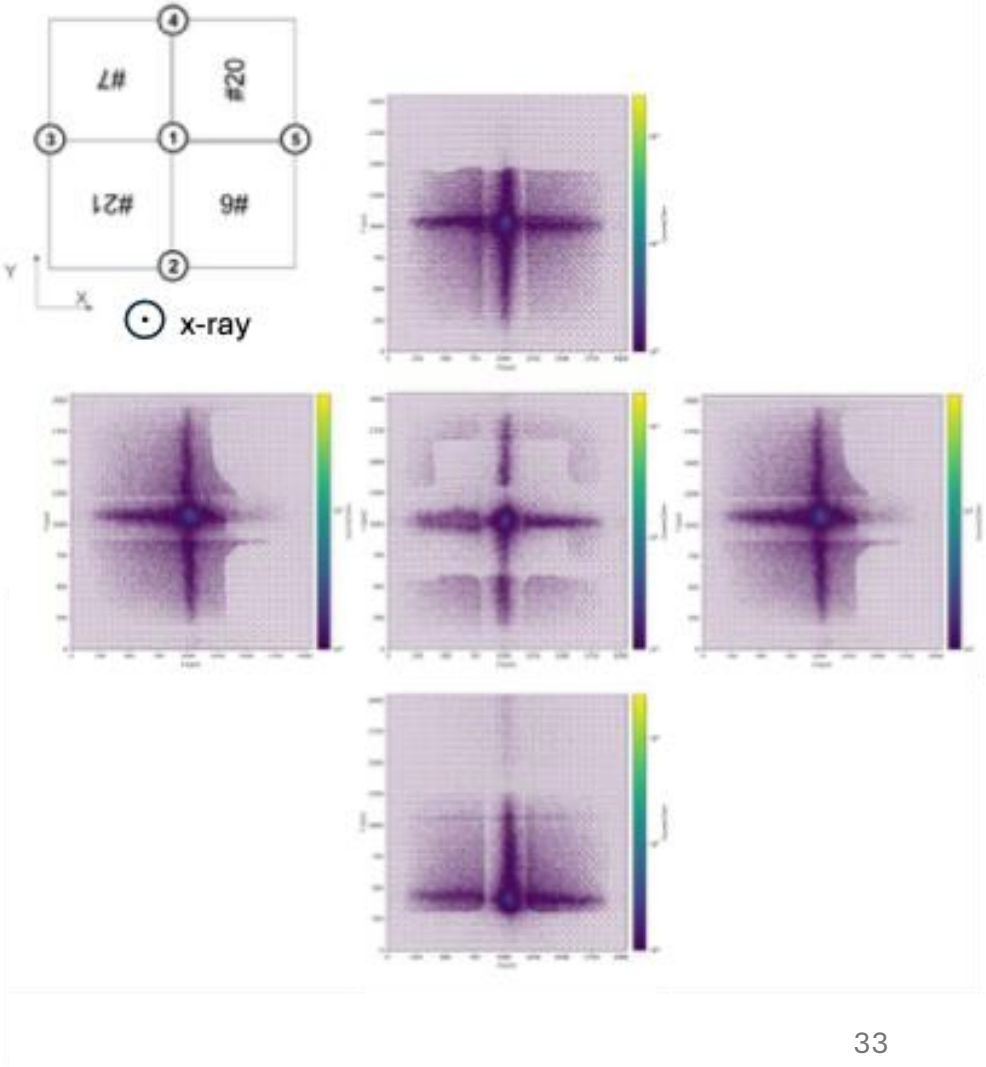

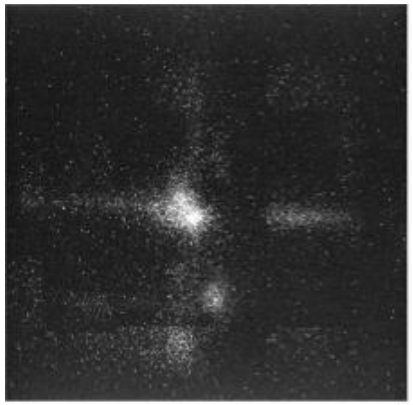

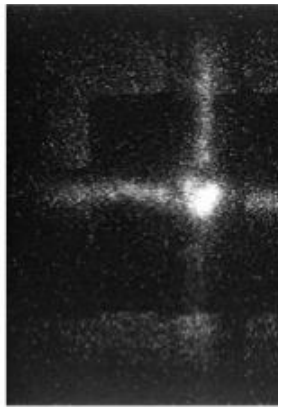

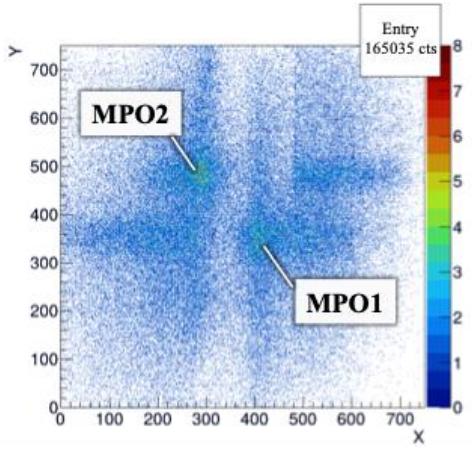

Setup and Frames